ENERGY-BALANCE EQUATIONS FOR IN-ROLL STRESSES FOR ANISOTROPIC MATERIALS IN WOUND ROLLS

by

Wadood Y. Hamad, B.Sc.

A Thesis submitted to the Faculty of Graduate Studies and Research in partial fulfilment of the requirements for the degree of Master of Engineering.

Department of Mechanical Engineering,
McGill University,
Montreal, Quebec
Canada.

 July, 1991.

'One basis for life and another
for science is a priori a lie.'

To

My beloved parents, aunt, uncle Tareq, Avis and my wonderful cousins Nadia, Sara and Zaid; for their kindness, support, in every sense of the word, and continued encouragement over the years which have been unparallelled.

ABSTRACT

This Thesis concerns itself with the thorough investigation of the effects of core material parameters on the structural behaviour of wound rolls in core-roll winding systems. The underlying theme in this work is the derivation, based on the theory of elasticity, of an analytic expression for the core material's elasticity modulus as a function of only material parameters and geometry.

The approach undertaken herein is purely theoretical and encompasses the rigorous analysis of principally two models; linear isotropic and anisotropic. As for the former, both planar and axisymmetric geometries are investigated; and in the case of the anisotropic model, an axisymmetric plane stress situation is studied. Moreover, finite-element modelling and analysis for the isotropic condition is carried out to confirm the theoretical findings. The objective is then to apply the results; namely, the inclusion of Poisson's ratio and elasticity modulus of the core material, to modify existing energy-balance roll structure formulae. This undertaking is called for if the aim is to have a valid winding model that simulates the actual winding process; i.e., one which incorporates sensing the presence of the core through layers of wound material. Results are further compared with existing winding models and conclusions are given.

RÉSUMÉ

La thèse presentée ci-dessous est impliquée dans l'enquête sur les effets des paramétres du matériel central sur le comportement structural des rouleaux. D'abord, le théme fondamental dans ce travail est celui de la dérivation, basée sur le théorie d'élasticité, d'une expression analytique pour le module d'élasticité du matériel central en fonction seulement des paramétres de la substance et de la géométrie.

La façon d'aborder cet ouvrage est tout à fait théorique. Celui-ci contient l'analyse rigoureux de deux modéles principales. Il s'agit de l'isotropie et de l'anisotropie linéaires. Le premier modél addresse les géométrie de surface plane et d'axisymmétriques. Quant au deuxiéme, celui d'anistropie un plane de contrainte axisymmétrique est recherché. En plus, le modél d'élément défini et l'analyse des conditions isotropiques sout recherchés afin d'affirmer les constatations théoriques. L'objective est alors d'appliquer les résultats; essentiellement, l'inclusion de rapport de Poisson et le module d'élasticité de la substance centrale pour improviser les formules existantes sur l'énergie-équilibre de la structure des rouleaux. Cette hypothèse est mise en jeu au cas ou le but sera d'obtenir un modél valable d'enroulement qui stimule la vraie façon d'enroulement; c'est-à-dire un modéle qui incorue la perception de la présence du noyau à travers des couches du matériel enroulé. Les résultats sout comparés davantage à d'autres modéles d'enroulement et des conclusions sout marquées.

FORWARD

The science of building good rolls has undergone some fundamental advances through the years. Proper winding of flexible sheet-like materials into rolls is an area in the field of mechanics which has broad utility in a number of diverse and important industries and which, therefore, has been of considerable interest over the past few decades.

The prime concern of this Thesis centres on how the stiffness of the core material in the core-roll winding system determines how much support it will offer for the initial wraps of web material, and whether this support will be maintained as internal pressures are developed.

The body of the Thesis is structured into three main parts. The first part, Chapter One, offers a brief literature review of existing theories for core-roll winding systems. An in-depth look is, however, taken at studying the energy-balance technique postulated by J. D. Pfeiffer; and several relevant examples are presented. Chapter Two, the essence of the theoretical work of this Thesis, consists of a thorough theoretical investigation of the core effects. It starts by investigating linear, isotropic materials via three different models. The first model being the linear, planar sheet-stack model; the other two, both axisymmetric, are thick-walled cylinder and press-shrink-fit models, used in analysing the hollow core problem. An independent finite-element analysis of the

linear, isotropic condition is further carried out and the outcome is reported. The latter segment of Chapter Two delves into the anisotropic analysis of the core-roll winding system. Initially, a detailed study of the theory of curvilinear anisotropy and generalised plane stress analysis for a body possessing cylindrical anisotropy is presented. Then a particular situation, the hollow-core problem, is modelled as an annular plate; and a detailed, rigorous analysis which results in expressions for stresses and deflections is carried out. The analysis is, moreover, expanded to encompass sensing the presence of the core through layers of wound material. All the theoretical findings of this Chapter channel into determining an analytic relationship for the effective elasticity modulus of the core material in the core-roll winding system. Several examples are given along the way to graphically demonstrate the significance of the theoretical findings. Comparison between results from the different approaches is presented, and conclusions pertaining to the universal applicability of each model are discussed.

Subsequently, these theoretical findings are implemented in modifying Pfeiffer's existing energy-balance roll structure formulae. This particular Chapter was the subject of a recent scientific publication entitled, "How Core Stiffness and Poisson Ratio Affect Energy Balance Roll Structure Formulas," by the author of this Thesis and his

supervisor, Professor J. D. Pfeiffer; which was presented at the First International Conference on Web Handling, held at Oklahoma State University.

The Thesis ends with a section bearing the titles, "Claims to Original Research" and "Suggestions for Further Work."

ACKNOWLEDGEMENTS

The author wishes to express his sincere gratitude and immense thanks to his supervisor, Professor J. David Pfeiffer, whose support, encourgement and guidance throughout the course of the research have been valuable and essential in ensuring worthwhile results. Thanks are further due for the provision of financial assistance through a research assistantship from a Natural Sciences and Engineering Research Council (NSERC) grant.

The author wishes to extend his most sincere thanks to his good friends; Dr. Hassan al-Kaisi, Mrs. Kathy al-Kaisi, Dr. Ali Shikara and Mr. Rafid Yousif, for their continued support notwithstanding the vast distances which separate them from the author. Last but not least, thanks are in order to Miss Wafa Harrouq, for her help in formulating the French version of the abstract.

TABLE OF CONTENTS

LIST OF ILLUSTRATIONS

LIST OF TABLES

NOMENCLATURE

Symbol		Dimension
P	inter-layer pressure	$MT^{-2}L^{-1}$
K_1	constant pressure multiplier	$MT^{-2}L^{-1}$
K_2	constant basic springiness factor	dim'less
K_3	constant strain multiplier	$MT^{-2}L^{-1}$
ε_r	radial compressive strain	dim'less
ξ_r	work done per unit volume in compressing a sheet of material from zero to a finite pressure of finite compressive stain	$MT^{-2}L^{-1}$
σ_w	web wound-in tension	$MT^{-2}L^{-1}$
ξ_w	elastic strain energy, per unit volume, in the roll resulting from the web wound-in tension	$MT^{-2}L^{-1}$
E_Θ, E_t	tangential elasticity modulus	$MT^{-2}L^{-1}$
E_r	radial elasticity modulus	$MT^{-2}L^{-1}$
σ_t	tangential stress	$MT^{-2}L^{-1}$
σ_r	radial stress	$MT^{-2}L^{-1}$
r	radius to a point in the finished roll	L
T	tension in the web	MT^{-2}
δ	web thickness (caliper)	L
ξ_t	energy per unit volume stored in the roll as a result of the tangential stress	$MT^{-2}L^{-1}$
ξ_s	total energy per unit volume stored by the roll stresses	$MT^{-2}L^{-1}$
σ_e	equivalent winding stress	$MT^{-2}L^{-1}$

Symbol		Dimension
σ'	- von Mise's equivalent stress	$MT^{-2}L^{-1}$
L_β	- fractional change in height of the wound-material-like sheets (denoted by α) used in the Linear Stack Model	dim'less
L_α	- fractional change in height of sheets possessing core material properties (denoted by ß) used in the Linear Stack Model.....	dim'less
E_c	- core material's elasticity modulus	$MT^{-2}L^{-1}$
ε	- total strain of entire sheet stack in the Linear Stack Model	dim'less
P_t	- tangential stress ($=\sigma_t$)	$MT^{-2}L^{-1}$
P_c	- radial stress ($= -\sigma_r$)	$MT^{-2}L^{-1}$
ε_1	- longitudinal principal strain	dim'less
μ	- Poisson's ratio	dim'less
E	- elasticity modulus	$MT^{-2}L^{-1}$
C_1, C_2	- constants	dim'less
ε_t	- tangential strain of the core outer surface.....	dim'less
a	- cylinder's inside radius	L
b	- cylinder's outside radius	L
p_i, p	- internal pressure	$MT^{-2}L^{-1}$
p_o, q	- external pressure	$MT^{-2}L^{-1}$
Δ	- change in radius of the hollow core	L

Symbol		Dimension
E_{eff}	- effective modulus of elasticity of the core material	$MT^{-2}L^{-1}$
μ_Θ	- Poisson's ratio in the tangential direction	dim'less
R_e	- modular ratio ($=E_{eff}/E$)	dim'less
α	- radial ratio	dim'less
β	- core thickness ratio ($=1-\alpha$)	dim'less
a	- core inner radius (finite-element model)	L
b	- core outer radius (finite-element model)	L
d	- roll outer radius (finite-element model)	L
u_b	- radial deformation at b	L
u_d	- radial deformation at d	L
p	- test pressure	$MT^{-2}L^{-1}$
ε_r, ε_Θ, ε_z, $\gamma_{\Theta z}$, γ_{rz}, $\gamma_{r\Theta}$	- components of deformation in the generalised Hooke's law	dim'less
σ_r, σ_Θ, σ_z, $\tau_{\Theta z}$, τ_{rz}, $\tau_{r\Theta}$	- stress components on planes normal to cylindrical coordinates r, θ, z	$MT^{-2}L^{-1}$
a_{ij}	- elasticity constants	$M^{-1}T^2L$
R, T, Z	- body forces per unit volume in coordinate directions r, θ, z	$MT^{-2}L^{-2}$
h	- plate thickness	L
u_r, u_Θ	- displacements in r and θ directions	L

Symbol		Dimension
σ_r^*, σ_θ^*, σ_z^*, $\tau_{r\theta}^*$	- averaged (with respect to thickness) stress components	$MT^{-2}L^{-1}$
u_r^*, u_θ^*	- averaged (w.r.t. thickness) displacements	L
$\mathbf{R}^*$, $\mathbf{T}^*$	- averaged (w.r.t. thickness) body forces.	$MT^{-2}L^{-2}$
ε_r^*, ε_θ^*, $\gamma_{r\theta}^*$	- averaged (w.r.t. thickness) components of deformation	dim'less
$U(r,\theta)$	- potential function	$MT^{-2}L^{-1}$
$U^*(r,\theta)$	- averaged (w.r.t. thickness) potential function	$MT^{-2}L^{-1}$
$F(r,\theta)$	- stress function	$MT^{-2}L^{-1}$
c	- radial ratio	dim'less
k	- anisotropy ratio	dim'less
A, B, C, D	- constants used in defining the stress function	dim'less
q_b, p_b	- pressure developed at core/roll interface	$MT^{-2}L^{-1}$
γ	- multiplier	dim'less
F_1, β, θ	- quantities used in determining γ	dim'less
R	- ratio of core to roll radii	dim'less
P_0	- "no-core" pressure	$MT^{-2}L^{-1}$
N_1-N_5	- empirical constants	dim'less
A_0	- constant used in the polynomial series expression for the radial modulus	$MT^{-2}L^{-1}$

Symbol		Dimension
A_1	- constant used in the polynomial series expression for the radial modulus	dim'less
A_2	- constant used in the polynomial series expression for the radial modulus	$M^{-1}LT^2$

CHAPTER ONE

BRIEF REVIEW OF EXISTING THEORIES FOR CORE-ROLL WINDING SYSTEMS

1.1 GENERAL INTRODUCTION

Webs are sheet materials that are sufficiently thin to produce negligible bending stresses when they are wound into rolls. Paper, magnetic tape, plastic wrap, photographic film base, adhesive tape and metal foils are common examples. Webs are wound into rolls for processing, transport and storage. Controlling in-roll stresses is important to prevent damage to the web due to excessive plastic deformations within the roll and to provide rolls that are sufficiently robust to withstand shock during transport.

The quality of a wound roll is dependent on the stresses which exist in it. Thus, in-roll stresses determine the structural integrity of the wound roll and make it an effective package for the web. These same in-roll stresses can, under certain conditions, impart damage to the web. Existing literature enables predicting the in-roll stresses developed by a specified winding tension. This stress state can then be examined to determine if it falls within the window of stresses that will yield a robust roll without damaging the web. If the stresses fall outside this window, the winding tension term in the existing winding models must be varied in a trial-and-error manner to attempt to produce an acceptable in-roll stress state.

The rigorous analysis of predicting wound roll

stresses resulting from a known winding tension, assuming that the coiled web exhibits constant orthotropic material properties, started with the work of Altmann [14] in which he derived exact integral expressions for the internal stresses from basic stress-strain relationships, based on the simplifying assumption of linearity in the radial-direction modulus of the wound roll. Earlier on, Tramposch [18] developed equations, using finite-difference methods, to predict the relaxation of internal stresses of a wound reel of magnetic tape, assuming a homogeneous and isotropic material which, under shear, exhibits instantaneous elasticity, delayed elasticity and creep; and under hydrostatic stressing shows elastic behaviour. He further extended his theoretical analysis to include the effect of a difference in the thermal properties of the tape and the hub [19].

An alternate, continuous solution for isotropic rolls by modelling the effect of the input tension through a modified expression for the circumferential strain, was suggested by Yablonskii [42]. Urmanskii et al. [38] expanded the latter solution to orthotropic rolls.

Yagoda [22] developed series solutions for integrals within Altmann's linear in-roll stress formulae. He then completed these solutions for winding tensions that are expressible as power series of the winding radius, through an accurate treatment of the core boundary conditions [23].

Yagoda extended the Altmann formulae for use with surface-wound rolls by dividing the roll into a thin outer section where inter-layer slip is allowed and a base where inter-layer slip is prohibited; however, the state of stress at the interface of the sections must be known to apply the results.

A comparison of the Altmann and Tramposch winding models was given by Connolly and Winarski [28]; moreover, they presented experimental data for stresses within reels of magnetic tape and analytically studied the effect of varying several winding parameters and temperature on the in-roll stresses.

Pfeiffer [1] experimentally demonstrated substantial non-linearity in the radial modulus of paper rolls. He then used his experimentally-determined radial stress-strain profile for paper as the basis of a continuous energy-based solution [5,6]. Furthermore, Pfeiffer [1] had previously described experiments for determining the stress state within finished rolls of paper. Experimental measurements of residual tension in a paper roll during unwinding by looping the uppermost layer of the roll over a force-sensing idler were performed and presented in a publication by Pfeiffer [3]. Hussain et al. [33] also presented in-roll stress data obtained from active sensors wound in to paper rolls.

Hakiel [15] extended the previous analysis of Altmann

by treating both the boundary conditions and the non-linear behaviour of the wound roll in a rigorous way, resulting in a computer model that is accurate enough to be used for simulation. Results obtained with Hakiel's model illustrated the highly non-linear nature of the winding process and compared well with experimental findings. Willett and Poesch [25] arbitrarily varied the radial modulus as a function of inter-layer pressure, as in Hakiel's model, in finite-difference models of the roll similar to that developed by Tramposch. They modelled winding the final roll by adding a sequence of layers of web. Willett and Poesch iterated to converge to a consistent set of inter-layer pressures and radial moduli for each layer added, while Hakiel avoided iteration by using a set of radial moduli computed from the inter-layer pressure distribution of the previously added layer.

An analytical comparison of the Pfeiffer [5,6], Hakiel [15] and Altmann [14] solutions was presented by Penner [16].

Several authors discussed the importance of controlling winding tension to obtain in-roll stresses sufficiently high to yield robust rolls but sufficiently low to avoid damaging the web within the roll. Harland [31] presented an analytical comparison of isotropic rolls wound with constant tension and constant torque. Frye [29] suggested a radial stress profile to avoid winding defects

in paper rolls and machine parameters that may affect the actual profile. Rand and Ericksson [34] recommended an in-roll stress distribution for newsprint on the basis of their analysis and experiments for determining in-roll stresses. Hussain and Farrel [32] experimentally determined the importance of controlling the winding tension at the start of a newsprint roll for avoiding loose cores.

An inverse solution, i.e., solving for the winding tension necessary to produce a desired residual stress distribution, was first demonstrated for isotropic rolls of wire by Southwell [37]. Whereas Catlow and Walls [27] derived the isotropic inverse solution for the winding tension necessary to obtain a constant residual tension in rolls of yarn wound on rigid cores. Since then, very little work has been done as regards the generation of prescribed residual stresses by solving for winding tension.

1.2 THE ENERGY-BALANCE APPROACH

1.2.1 Background

When rolls of paper, film, plastic sheeting, or other thin flexible webs are wound, it is of interest to know what stresses exist in the roll, both during and after winding. If we know these stresses and how they may be changed by varying the winding tension and other parameters, the causes of many roll defects and their cures may also be known.

Roll structure theory has been successful in describing the relationship between internal stresses in a finished roll and the stresses that exist on the surface as the roll is being wound. This relationship is important in that it allows us to relate different types of experimental tests to each other. It also allows us to monitor on-line such properties as wound-in tension, wound-off tension and roll density rather than having to perform destructive off-line testing of finished rolls [16].

In essence, roll structure theory has been developed in three stages. Altmann derived a relationship between internal stresses and the wound-in tension for an anisotropic model in which all stress-strain relations were linear [14]. The solution was basically analytical in nature, with only one numerical integration required to apply the relevant formulae. Pfeiffer [5,6] extended the analysis to deal with non-linear behaviour in the radial

direction, perpendicular to the sheet. This theory involved the numerical solution of a single, first-order, non-linear differential equation. The solution procedure was simplified by assuming an energy balance on a single wrap of paper as a function of time. On the other hand, Hakiel [15] extended Altmann's original work to deal with the general non-linear problem without making any specific energy-balance assumptions. In all of the aforementioned work, Poisson's ratio was assumed to be negligible and hence was not included into the analyses.

1.2.2 Pfeiffer's Energy-Balance Roll Structure Formulae

Authors [14, 34, 36, 18, 19] have, in their attempts to calculate the roll structure, acknowledged the non-linear compression behaviour of paper and films in the direction perpendicular to the plane of the sheet but, nonetheless, opted to use a linear modulus in their final solutions. In cases where the variation in tension is inversely proportional to the roll radius, as in centre-winding, or in cases where there is no variation, the linear modulus approach can give a closed-form solution to the distribution of inter-layer pressure and residual tension versus radius [5]. However, when the pattern of tension wound into the roll is not a simple function of radius, these solutions must be evaluated numerically. Pfeiffer's work [5,6] takes a different approach to the

problem and applies energy-balance techniques to help solve the non-linear compression case.

It is essential to deal with non-linear compressibility since the latter is tantamount to the observed stress-strain behaviour of stacks of sheet material. It has been determined [1,2] that paper follows the relationship:

$$P = -K_1 + K_1 \exp(K_2 \varepsilon_r), \qquad (1.1)$$

where, P = radial stress (inter-layer pressure), in Pa or psi,

K_1 = pressure multiplier, in Pa or psi,

K_2 = basic springiness factor, dimensionless, and

ε_r = radial compressive strain, dimensionless.

It is worthwhile noting that the quantity K_2 forms the basis for the exponential sweep of the curve of equation (1.1). For soft, high-bulk materials, it is low, in the range 6-15; indicating a low change of pressure with strain. With most printable grades of paper, K_2 falls between 15 and 100. Very hard, dense products and homogeneous plastic films are characterised by a K_2 of 100-500 [7].

The reason for this behaviour in fibrous materials was demonstrated by Elias [50]. By a similar line of reasoning, one can explain why homogeneous materials; such as plastic film, also follow an exponential relationship as the point of contact or support between adjacent sheets

come closer together with increasing pressure [5].

When compressing a stack of sheet material from zero pressure to a finite pressure or a finite compressive strain, the work done per unit volume is equal to the area under the stress-strain curve from zero up to that point. Hysteresis is involved with actual materials, indicating that more energy is required to compress than will be released on expansion. Pfeiffer managed, in his approach [5,6], to side-step this problem by defining K_1 and K_2 to match the relaxing behaviour only. Hence, the area under the stress-strain curve is obtained by integrating equation (1.1); i.e.,

$$\xi_r = \int_0^{\varepsilon_r} -K_1 d\varepsilon_r + \int_0^{\varepsilon_r} K_1 \exp(K_2 \varepsilon_r)\, d\varepsilon_r = \frac{P}{K_2} - \left(\frac{K_1}{K_2}\right) \ln\left[\frac{P}{K_1} + 1\right], \quad (1.2)$$

where, ξ_r, in J/m^3, is the energy involved in compressing the roll material up to the radial strain ε_r; and other symbols are as defined earlier.

There is a steady supply of available energy coming to the roll in the form of elastic strain in the web because of its wound-in tension, σ_w (in units Pa or psi). The magnitude of this energy input, denoted by ξ_w, per cubic volume unit is given by:

$$\xi_w = \sigma_w^2/(2E_t), \quad (1.3)$$

where ξ_w is in units of J/m^3 and E_t, the tangential modulus

of the roll, in Pa or psi. On the outside of the roll, where the residual tension is positive and the pressure low, most of this energy will be tensile in nature. Interior sections of the roll, which used to be on the outside, have been compressed radially, and the residual tension has been reduced. In these sections, most of the energy from σ_w has been converted into compressive energy. One of the premises of Pfeiffer's energy-balance approach is that the tension disturbances or variations stay close to the location at which they occurred. This is substantiated by measurements of wound-in tension [4], in which small disturbances made within one or two revolutions of the winding roll can be played back and found to be in the same place they were made.

Most of the energy of wound-in tension applied to the roll will find its way into radial compressive energy. This makes the cylindrical roll body firm and allows it to be transported more readily than a stack of sheets [5].

All solutions to roll structure problems must satisfy the elastic equilibrium requirements of sections of the roll; namely,

$$\sigma_t - \sigma_r - r(d\sigma_r/dr) = 0, \qquad (1.4)$$

where, σ_t = tangential stress, in Pa or psi,

σ_r = radial stress, in Pa or psi, and

r = radius to a point in the finished roll, in metres or inches.

Here, the tangential stress is related to the tension, T, in N/m or pli (pounds per lineal inch) via,

$$\sigma_t = T/\delta, \tag{1.5}$$

where, δ designates the web thickness (usually referred to as the caliper) in micro-metres or inches.

The difference between the various solutions to the roll structure problem stems from how the interrelation between σ_w, σ_t and σ_r has been defined. Let us assume that the energy of a single wrap is conserved as a function of time as the roll is built. That is, there is no energy transfer between successive wraps in the roll. The energy in a wrap is known when it is first put on the roll and is given by equation (1.3). As the wrap becomes an internal layer, this energy gets transformed from pure tensile energy into a combination of compressive energy (radial) and some residual tensile energy (tangential), but the energy of this wrap is still conserved. The question is, which energy?

Pfeiffer [5,6] postulates that it is von Mises' distortion energy that is conserved rather than the total energy stored by the roll stresses, ξ_s, given by:

$$\xi_s = \xi_r+\xi_t = \xi_r+[\sigma_t^2/(2E_t)], \tag{1.6}$$

where ξ_r has been defined in equation (1.2). The distortion energy is defined as the portion of the total energy associated with the a change in shape of a body rather than a change in volume. By assuming it is conserved, we

obtain:

$$\xi_w = \xi_r \pm (\xi_r \xi_t)^{1/2} + \xi_t. \qquad (1.7)$$

Note that (±) preceding the middle term is inserted in order to accommodate for the situation when σ_r is negative and σ_t positive, hence resulting in the energy term being higher than when σ_r and σ_t have the same sign. Pfeiffer's method [5,6] seemingly tends to reduce the error between the locally applied energy, given by equation (1.3) and the total energy stored by the roll stresses, given by equation (1.6). Upon substituting equation (1.7) into equation (1.4) and making use of the boundary condition σ_r=0 at the roll outer radius (which is constantly changing); Pfeiffer's solution is obtained.

It is noteworthy that shear stresses are neglected since the roll is assumed to be symmetrically circular [5]. The bending stresses to wrap each layer around the rest of the roll are also neglected for most thin-gauge materials. However, for thick materials, the energy to bend on a per-unit-volume basis may be compared with the winding stress energy to see if it may be disregarded. Hitherto, Poisson's ratio has not been brought into the analysis. It will be shown in Chapters Two and Three how Poisson's ratio can be incorporated in the analysis of roll structure.

Focussing our attention on the method of solution, the procedure used is to find a winding stress, σ_e, that has an energy level equivalent to the local pressure. This is

achieved by multiplying ξ_r by $(2E_t)$ and taking the square root of the product. I.E.

$$\sigma_e = -\{2E_tP/K_2 - (2E_tK_1/K_2)\ \ln[(P/K_1)+1]\}^{1/2}. \qquad (1.8)$$

The distortion energy theory [6] is then used to obtain von Mises' equivalent stress, σ', from the compression equivalent stress, σ_e, and the residual tensile stress, σ_t, as follows:

$$\sigma' = (\sigma_e^2 - \sigma_e\sigma_t + \sigma_t^2)^{1/2}. \qquad (1.9)$$

This distortion energy all comes from the winding stress, σ_w, so if σ' is set equal to σ_w and we solved quadratically; σ_t can be obtained, and from that, into equation (1.4) we can find $r(d\sigma_r/dr)$. That is,

$$\sigma_t = 0.5\{-\sigma_e + (-3\sigma_e^2+4\sigma_w^2)\}, \qquad (1.10)$$

$$r(d\sigma_r/dr) = -\sigma_t - \sigma_r, \qquad (1.4')$$

where $(d\sigma_r/dr)$ is the rate of change of pressure with radius.

1.2.3 Winding Examples

The author has managed, making use of the algorithm[1] based on the energy-balance technique that enables us to predict the roll structure under a given pattern of wound-in tension; to produce some of the winding examples which appeared in a publication by Pfeiffer in 1979 [5].

Fig. 1.1a shows the variation of radial pressure (in

[1] The program in question is DPROL90.bas which is copyright December, 1990 by J. David Pfeiffer.

kPa) with radius for a 0.876-m-diameter roll of catalogue paper [1]. Whereas Fig. 1.1b illustrates the plots of residual tension and wound-in tension (both in N/m) versus radius for the same catalogue paper roll. The values used for K_1, the tangential modulus of the roll, E_t, and the caliper (web thickness), δ, were 2.3 kPa, 4820 MPa and 51μm; respectively.

Although equation (1.1), the basis of the current analysis, was developed to fit the non-linear compression behaviour of many materials, it may also be used to simulate the linear case as well if K_2 is kept low (in the range of about 2 to 5) and the product of K_1 and K_2 is adjusted to equal the linear compressive modulus, perhaps from 16 to 100 times smaller than the tensile modulus [5]. And, hence, a comparison of centre-winding with linear and non-linear moduli can be made, and it is shown in Figs. 1.2a,b and 1.3a,b; respectively. In the first set of figures pertaining to the linear modulus, K_1 and K_2 were 86,125 and 3.5, respectively. Whilst for the non-linear case, the constants were K_1=206.7 and K_2=190. For both, the tangential modulus of the roll was 4820 MPa and the web thickness 25.4 μm. Figs. 1.2a and 1.3a illustrate how the radial pressure varies with radial ratio, whereas Figs. 1.2b and 1.3b represent the variation of residual and wound-in tensions with radial ratio. The plots are actually four curves drawn on top of each other,

demonstrating a build-up ratio of 1.5, 2, 2.5 and 3 from the core.

a.

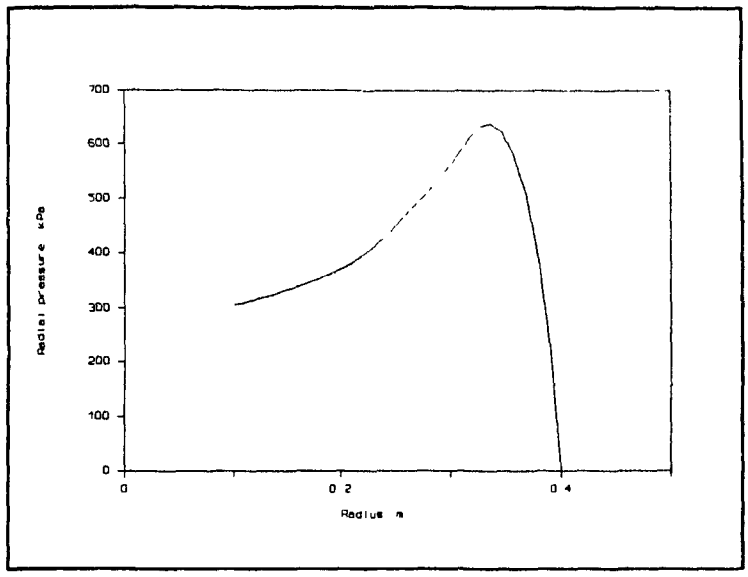

b.

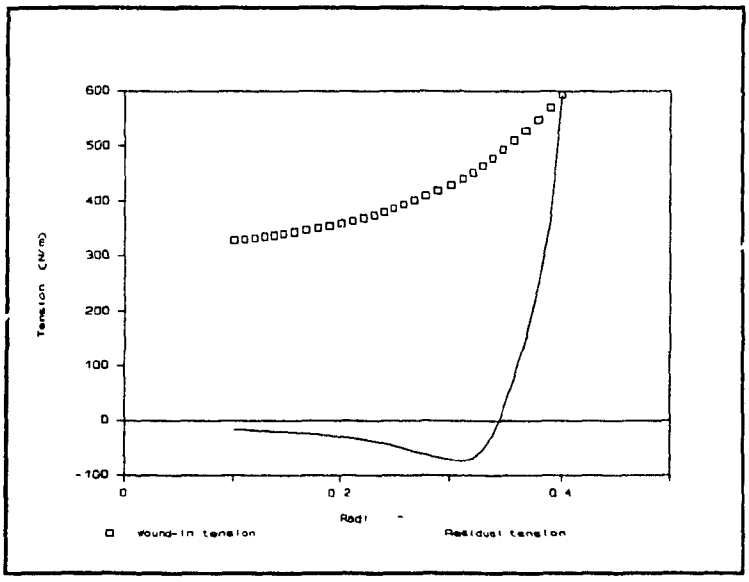

Fig. 1.1: Plots of radial pressure, residual tension and wound-in tension versus radius for a 0.876-m-diameter roll of catalogue paper, energy-balance solution.

a.

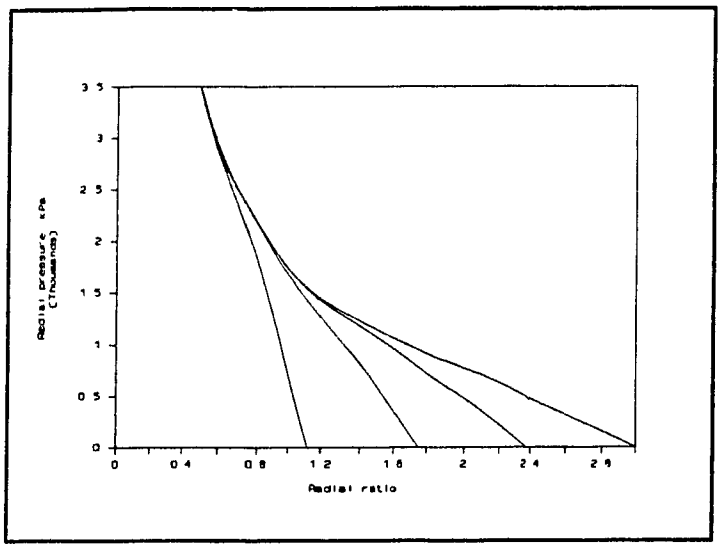

b.

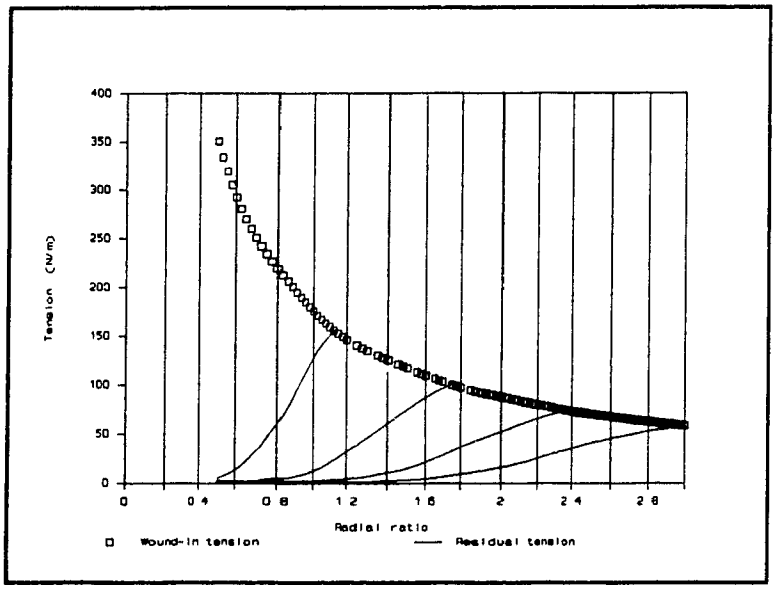

Fig. 1.2: Plots of radial pressure, residual tension and wound-in tension versus radial ratio for a centre-wound roll with a linear compressive modulus, energy-balance solution (constant winding torque).

a.

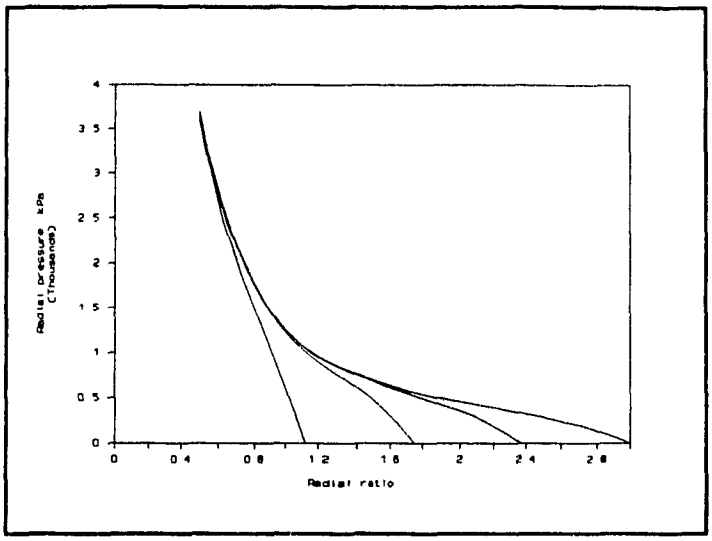

b.

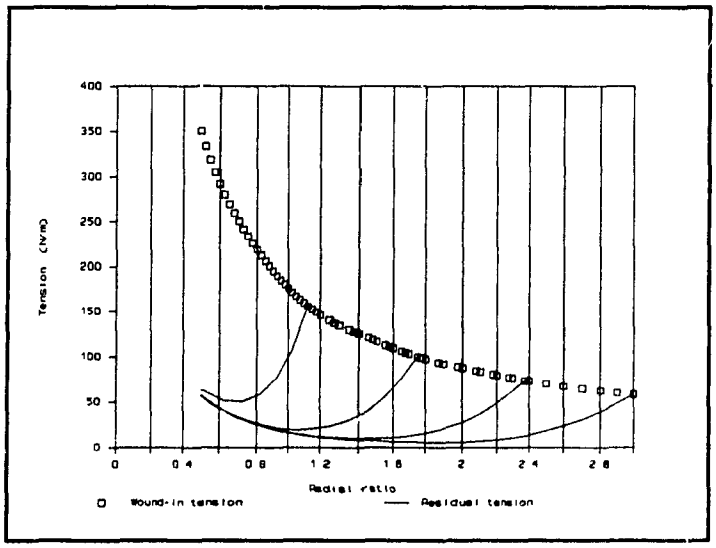

Fig. 1.3: Plots of radial pressure, residual tension and wound-in tension versus radial ratio for a centre-wound roll with a non-linear compressive modulus, energy-balance solution (constant winding torque).

CHAPTER TWO

EXAMINATION OF CORE EFFECTS

2.1 INTRODUCTION

Core characteristics play an important role in influencing the internal stresses of wound rolls . Hence, a clear understanding of the behaviour of the core material properties is paramount to predicting the effect of the core on the inter-layer pressure and wound-in tension of wound rolls of, for instance, paper.

In this chapter, a detailed investigation of how the core affects the roll material is provided. An attempt at predicting the effective elasticity modulus of the core material in the core-roll winding system is made, and the theoretical predictions are verified by a finite-element model. A thorough study of thick-walled cylinder theory is presented in the endeavour to pave the road for a clear understanding of its applicability to the problem at hand; namely, investigating the core effects on wraps of wound material in core-roll winding systems.

2.2 THE LINEAR STACK MODEL

2.2.1 Background

The first step taken in the endeavour to clearly understand the core material effects on the wound roll was to model the core-roll combination as a stack of sheets. The stack model is a linear model principally consisting of planar sheets layered horizontally one on top of the other (refer to Fig. 2.1). This linear-planar model obviously excludes any regards to the actual axisymmetric geometry of the core structure and, thus, provides only a rough approximation, at best, to the actual behaviour of the core material.

Initially, some certain percentage of the total number of sheets making up the stack model, say 99 percent, is taken to behave like the core material in question. The remainder is to have the properties of the material being wound round the core. Thereafter, each layer having the core properties is stripped and replaced by the winding material. This process is successively continued until all of the roll material sheets replace the core material.

2.2.2 The Mathematical Model

The mathematical equations governing the subject model can be developed from the basic equation describing the non-linear behaviour of paper [1, 2, 5]; viz.,

$$P = -K_1 + K_1 \exp(K_2 \varepsilon_r), \quad (2.1)$$

where, P = radial stress, Pa or psi,

K_1 = pressure relation multiplier, Pa or psi,

K_2 = basic springiness factor, dimensionless, and

ε_r = compressive strain, dimensionless.

By algebraically manipulating the previous equation we get,

$$\varepsilon_r = \{\ln(P/K_1 + 1)\}/K_2, \quad (2.2)$$

and further using α, a fraction of unity (noting here that unity is the total sheet stack height), to designate the portion of the layers experiencing direct core effect (i.e. sheets having core material properties) and the fact that $\beta=1-\alpha$ (see Fig. 2.1), equation (2.2) then becomes;

$$L_\beta = \{\beta/K_2\}*\ln(P/K_1 + 1),$$

$$L_\beta = \{(1-\alpha)/K_2\}*\ln(P/K_1 + 1), \quad (2.3)$$

where L_β is the fractional change in height of the wound-material-like sheets, and is dimensionless. Similarly, using L_α to denote the fractional change in height of the sheets having the core material properties, the equation used to define L_α is;

$$L_\alpha = \alpha*P/E_c, \quad (2.4)$$

where E_c is the modulus of elasticity of the core material, in the same units as P.

Then, the total strain of the entire sheet-stack arrangement, ε, will be

$$\varepsilon = L_{\alpha} + L_{\beta},$$

$$\varepsilon = \alpha * P/E_c + \{[(1-\alpha)/K_2]\ \ln(P/K_1 + 1)\}. \qquad (2.5)$$

Equation (2.5) describes the total strain of the two-component model as a function of the radial stress, modulus of elasticity of the core, respective heights of the wound-material and core-like sheets and, K_1 and K_2 pertaining to the wound-roll material. Thus, knowing an initial pair of values for K_1 and K_2 of the wound material, and the stiffness or modulus of the core, E_c, the stiffness of the two-part stack can be determined for a specific range of pressure values. The new relation between strain and pressure is then used to determine a new set of K_1 and K_2 values depending upon α and the relative amount of core material included.

2.2.3 Examples and Conclusions

In this sub-section we shall use the results of analysing three particular cases to draw conclusions so as to establish whether the linear stack model is a viable approach to accurately predicting how the stiffness of the core determines how much support it will offer for the initial wraps of web material.

Case One

The first case has the following roll and core material properties:

Roll;

$E_{tangential}$ = 600,000 psi (4.134 GPa),

$E_{radial}(P) = 1060*P - 0.153*P^2$, in psi,

$= 1060*P - (2.22\times10^{-5})*P^2$, in Pa, and

Poisson's ratio, $\mu = 0$.

Core;

E_{core} = 890,000 psi (6.132 GPa).

Case Two

As case one except for;

$E_{radial}(P) = 124*P$, in psi or Pa.

Case Three

All properties as in case one except for;

E_{core} = 8,900,000 psi (61.32 GPa).

For each of the above cases, since we have the radial elasticity modulus defined as a function of pressure[1], we can write a simple routine to compute the strains as a function of pressure, too. The strain-pressure values thus obtained can then be input into another routine[2] which uses equation (2.1) as the basis for determining, by way of re-iterative computations, the best pair of K_1, K_2 values for the particular situation under consideration. This pair of

---

1 The polynomial representation of E_r is the form used for handling the non-linear compression in the Hakiel model solution [15].

2 written by J. D. Pfeiffer.

K_1, K_2 values, which we shall call the initial pair, is thence used in equation (2.5) with the appropriate substitutions for E_c, α and a suitable range of P values; to compute the total strain of the entire sheet-stack arrangement.

Recalling that, in essence, the linear stack model constitutes the replacement of a sheet with some initial K_1, K_2 values with one having K_1, K_2 values determined from equation (2.5), the above-described procedure may be continued to find a pair of K_1, K_2 values corresponding to a certain α. Thus, continuing in this fashion one can put forth a prediction of how K_1 and K_2 vary with α. In other words, we should be able to know how quickly the core effect fades away.

The K_1, K_2 values corresponding to specific values of α obtained from the aforementioned calculations are plotted for the three cases under investigation (see Figs. 2.2 & 2.3). The numerical values are then used in a least-square-curve-fitting technique to come up with an equation that best describes the relationship between K_1, K_2 and α. It was found that best fit between K_1 and α, and K_2 and α may be represented by an exponential equation of the form,

$$Y = A*\exp(B*X) - C, \qquad (2.6)$$

where, Y represents K_1 or K_2,

X represents α, and

A, B and C are empirically determined constants.

Table 2.1 contains values for A, B and C for the three examined cases for both K_1 versus α, and K_2 versus α.

It becomes apparent, after the careful examination of the graphs and equations describing the relation between K_1 and α, and K_2 and α; that the linear stack model does not provide us with an adequate understanding of how the core effects tend to influence the wound material. This is true since it is noticed that as more roll material is added, the effect of the core does not fade away as quickly as one would intuitively expect. Moreover, the high degree of empiricism associated with arriving at equation (2.6) precludes one from expanding the results to more universal situations. This, indeed, is also due to the somewhat severe restrictions on the chosen model from the standpoint of the actual geometry pertaining to the core-roll system. We are therefore forced to abandon the linear stack model used hitherto and, endeavour to venture with an axisymmetric model.

Table 2.1: Summary of the numerical results for three particular cases, using the Linear Stack Model.

	$K_1 = A*\exp(B*\alpha) - C$		
	A	**B**	**C**
Case One	0.496088	1.34672	-0.583601
Case Two	0.101059	2.17807E-02	-1.30718E-05
Case Three	5.10060E-02	1.02927	-0.584226
	$K_2 = A*\exp(B*\alpha) - C$		
	A	**B**	**C**
Case One	10518.4	0.268348	6855.35
Case Two	528.873	0.943581	3.69185
Case Three	4626.75	0.876170	283.030

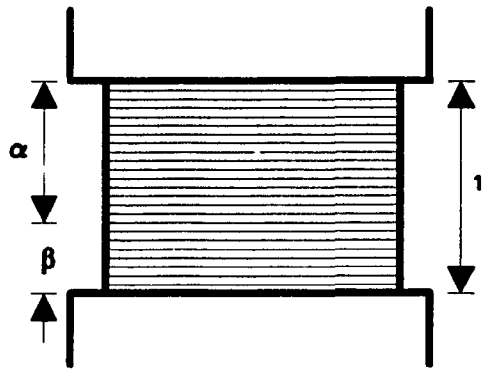

α = portion of layers experiencing direct core effects, and

ß = remaining portion exhibiting wound-material-like properties.

Fig. 2.1: The Linear Stack Model of the core material.

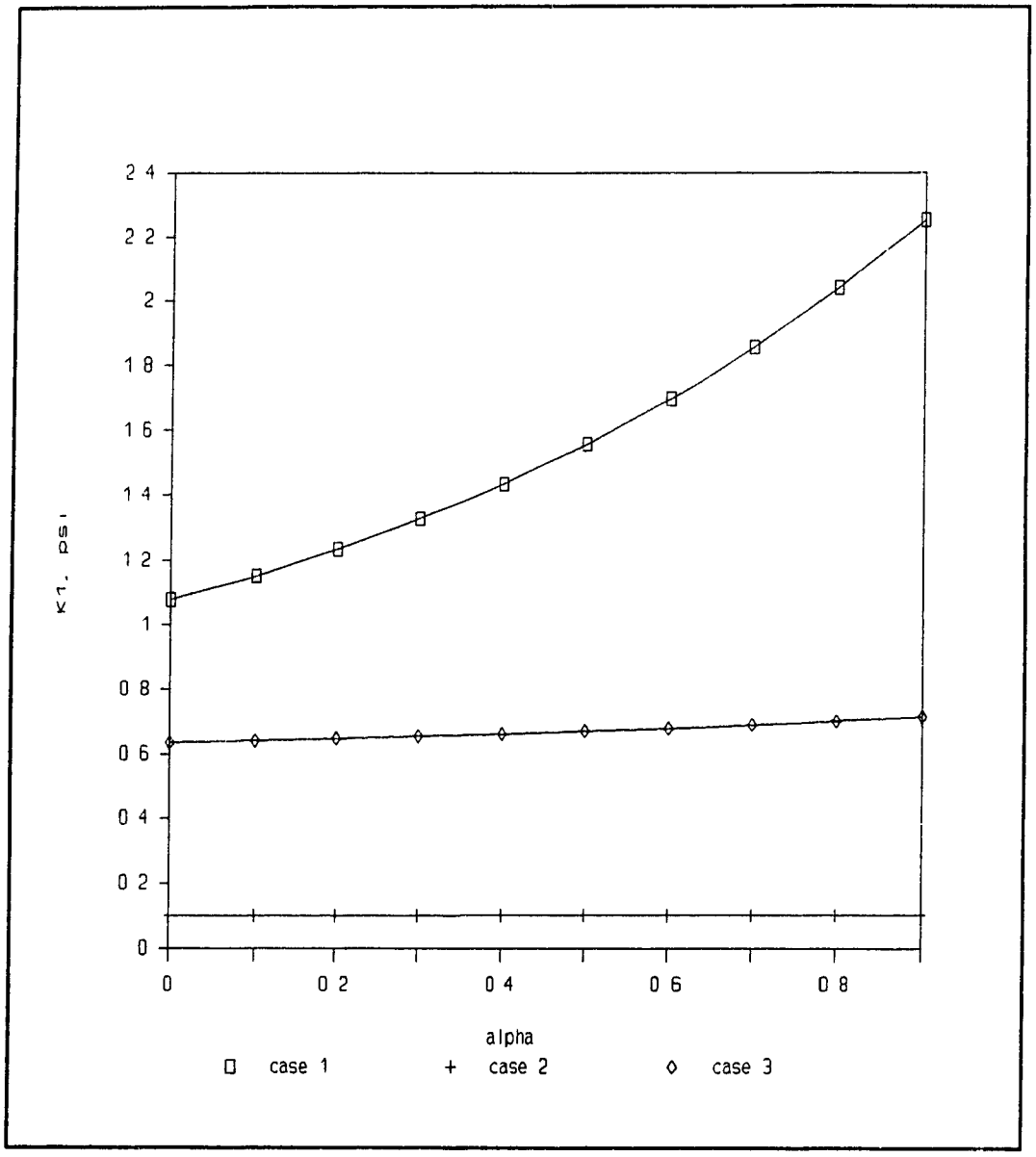

Fig. 2.2: Graph of K_1 versus α for three particular cases (described in sub-section 2.2.3), obtained from equation (2.6) of the Linear Stack Model.

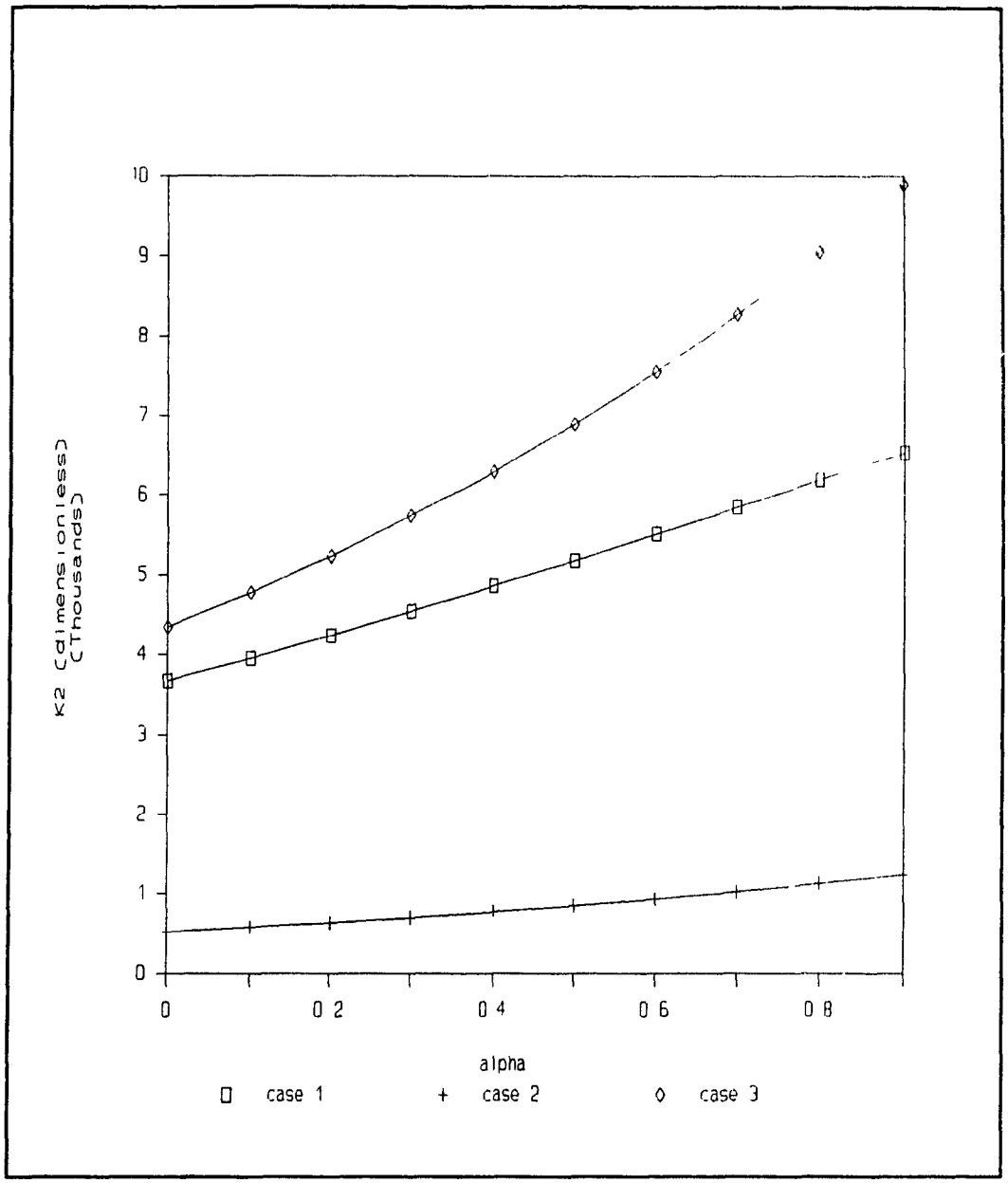

Fig. 2.3: Graph of K_2 versus α for three particular cases (described in sub-section 2.2.3), obtained from equation (2.6) of the Linear Stack Model.

2.3 THE AXISYMMETRIC MODEL

In an attempt to improve upon last section's findings we shall, thenceforth, modify the hitherto-studied model to include in the analysis the true geometry of the core-roll system. Thus, an axisymmetric model will be used to simulate the core-roll system. However, we shall continue our analysis, at this stage, to consider materials exhibiting isotropic behaviour. That is to say, that the material parameters; viz., Poisson's ratio, μ, and elasticity modulus, E, are the same in all directions. I.E., $\mu_{rt}=\mu_{tr}$ and $E_r=E_t$, where r and t represent the radial and tangential directions, respectively. The subscripts used in the notation pertaining to Poisson's ratio characterise a dimensional decrease in the direction of the second subscript during tension in the direction of the first subscript. Hence, in studying the isotropic condition, it should be apparent, whether μ and E are subscripted or not, that equivalence of the material parameters in both the radial and tangential directions is presumed.

The results procured from the analysis in this section are purely analytic, and the identity between the two approaches undertaken here on, the thick-walled cylinder analysis and the press-shrink-fit model, will be verified. An equation for predicting the effective core elasticity modulus for a hollow isotropic core is derived.

2.3.1 Thick-Walled Cylinder Analysis

2.3.1.1 Stresses in Thick-Walled Cylinders

A thick-walled cylinder subjected to external or internal pressure, or both, has radial and tangential stresses with values which are radius-dependent. A thick-walled cylinder may also be stressed longitudinally. In determining the radial and tangential stresses we make use of the assumption that the longitudinal elongation is constant around the circumference of the cylinder, i.e., a right section of the cylinder remains plane after stressing.

Referring to Fig. 2.4, we designate the inside radius of the cylinder by a, the outside radius by b, the internal pressure by p_i, and the external pressure by p_o. Sections of the cylinder must satisfy global static equilibrium requirements. Thus, considering the equilibrium of a thin semicircular ring cut from the cylinder at radius r and having a unit length (see Fig. 2.4); and setting the summation of forces in the vertical direction equal to zero, we have

$$2\sigma_t dr + 2\sigma_r r - 2(\sigma_r+d\sigma_r)(r+dr) = 0, \qquad (2.7a)$$

by further simplifying equation (2.7a) and neglecting higher order quantities, we obtain the familiar form commonly referred to as the hoop stress equation; viz.,

$$\sigma_t - \sigma_r - r(d\sigma_r/dr) = 0, \qquad (2.7b)$$

where; σ_t = tangential stress, in Pa or psi, and

σ_r = radial stress, in Pa or psi.

Defining P_t and P_c to be equal to σ_t and $-\sigma_r$, respectively, equation (2.7b) may be re-written equivalently as;

$$P_t + P_c + r(dP_c/dr) = 0, \qquad (2.7c)$$

which often appears in the literature.

We wish to obtain general expressions for σ_t and σ_r as functions of a, b, p_i and p_o. Equation (2.7b) relates two unknowns σ_t and σ_r, but we must obtain a second relation in order to evaluate them. The second equation is obtained from the assumption that the longitudinal deformation is constant. Hence, for the triaxial state of stress under consideration, the longitudinal principal strain will be:

$$\varepsilon_1 = -(\mu\sigma_t/E) - (\mu\sigma_r/E), \qquad (2.8a)$$

where, ε_1 = longitudinal principal strain, dimensionless,

μ = Poisson's ratio, and

E = modulus of elasticity of the cylinder, Pa or psi.

(**N.B.** Both, the tangential and radial stresses, are positive for tension.)

Proceeding with our objective of finding general expressions for σ_t and σ_r, we notice that equation (2.8a) can be rearranged, since ε_1, μ and E are constants; in the form

$$-E\varepsilon_1/\mu = \sigma_t + \sigma_r = 2C_1, \qquad (2.8b)$$

where C_1 is a constant. Next solving equations (2.7b) and (2.8b) to eliminate σ_t produces

$$r\, d\sigma_r/dr + 2\sigma_r = 2C_1. \qquad (2.9a)$$

Multiplying equation (2.9a) by r gives

$$r^2(d\sigma_r/dr) + 2r\sigma_r = 2rC_1. \qquad (2.9b)$$

However, noting that

$$d(r^2\sigma_r)/dr = r^2(d\sigma_r/dr) + 2r\sigma_r, \qquad (2.10)$$

$$\therefore \quad d(r^2\sigma_r)/dr = 2rC_1. \qquad (2.11a)$$

Integrating equation (2.11a) gives

$$r^2\sigma_r = r^2C_1 + C_2, \qquad (2.11b)$$

where C_2 is a constant of integration. Solving for σ_r from equation (2.11b) we obtain,

$$\sigma_r = C_1 + (C_2/r^2). \qquad (2.11c)$$

Substituting equation (2.11c) for σ_r into equation (2.8b), we find

$$\sigma_t = C_1 - (C_2/r^2). \qquad (2.12)$$

In order to evaluate the constants of integration C_1 and C_2, we need to make use of the boundary conditions of the cylinder. The boundary conditions are;

$\sigma_r = -p_i$ at $r = a$, and

$\sigma_r = -p_o$ at $r = b$.

Substituting these boundary conditions into equation (2.11c) yields;

$$-p_i = C_1 + (C_2/a^2), \qquad (2.13a)$$

$$-p_o = C_1 + (C_2/b^2). \qquad (2.13b)$$

The constants C_1 and C_2 can be found by solving equations (2.13a) and (2.13b) simultaneously. This gives

$$C_1 = (p_i a^2 - p_o b^2)/(b^2 - a^2), \qquad (2.13c)$$

$$C_2 = a^2 b^2 (p_o - p_i)/(b^2 - a^2). \qquad (2.13d)$$

Substituting the previous expressions for C_1 and C_2 into equations (2.11c) and (2.12), yields the sought general expressions for σ_t and σ_r as functions of a, b, p_i and p_o; namely,

$$\sigma_t = \frac{p_i a^2 - p_o b^2 - a^2 b^2 \dfrac{(p_o - p_i)}{r^2}}{(b^2 - a^2)} \qquad (2.14)$$

and,

$$\sigma_r = \frac{p_i a^2 - p_o b^2 + a^2 b^2 \dfrac{(p_o - p_i)}{r^2}}{(b^2 - a^2)} \qquad (2.15)$$

Equations (2.14) and (2.15) make possible the determination of the stress state inside a thick-walled cylinder subjected to external and/or internal pressures.

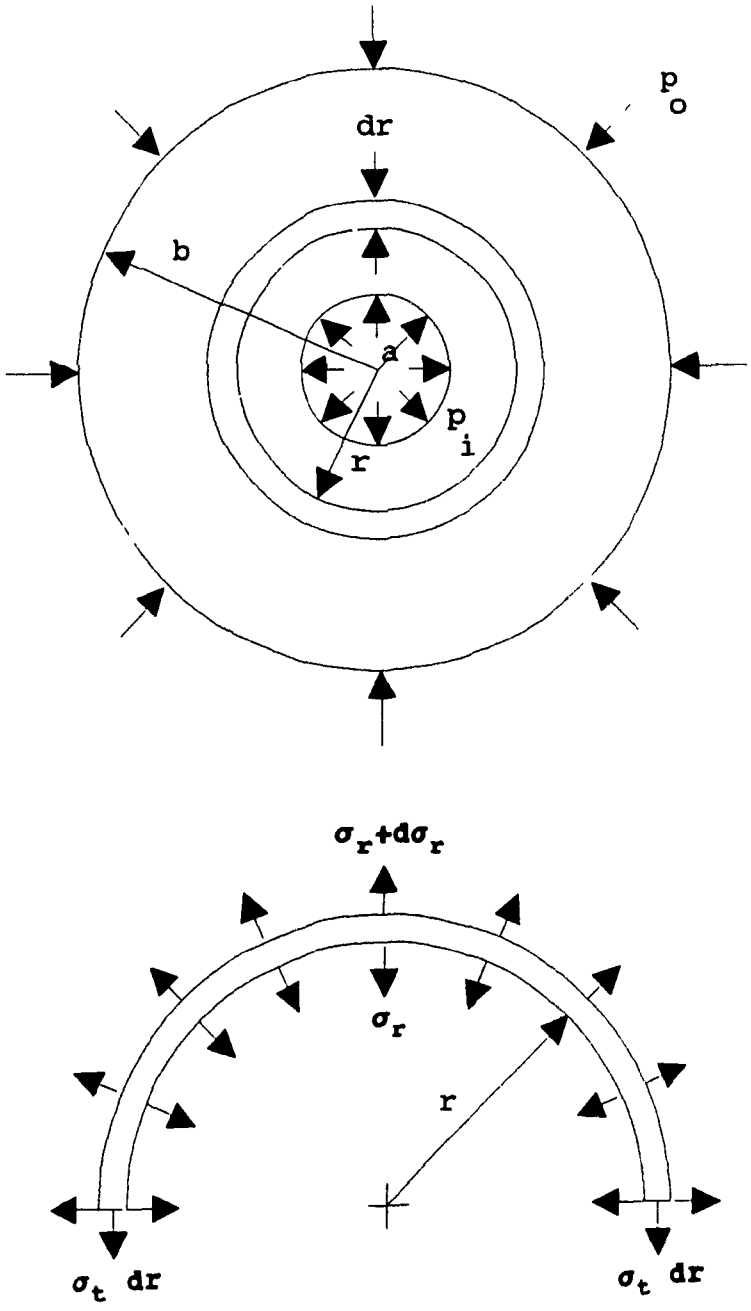

Fig. 2.4: Elements in a thick cylinder.

2.3.1.2 A Particular Case: An Isotropic Hollow Core

The thick-walled cylinder theory is applied to simulating the stresses and stiffness of the core material in the core-roll winding system. Hence, the results obtained from the thick-walled cylinder analysis will justifiably apply towards solving the issue of concern; namely, developing an analytic equation for predicting the effective elasticity modulus of an isotropic, hollow core.

Fig. 2.5 illustrates a hollow core with inner (hole) radius, a, outer radius, b, and uniform core pressure, p, developed by the wound-roll material surrounding the core. Denoting the change in radius of the hollow core by Δ and, the tangential strain of the core outer surface (at r=b) by ε_t we have,

ε_t = change in circumference/original circumference,

$\varepsilon_t = \{2\pi(b+\Delta) - 2\pi b\}/2\pi b$,

$\varepsilon_t = \Delta/b$,

or $\Delta = b\varepsilon_t$. (2.16)

However,

$$\varepsilon_t = (\sigma_t/E) - (\mu\sigma_r/E), \quad (2.17)$$

where μ and E are the core's Poisson's ratio and elasticity modulus, respectively. σ_t and σ_r, at the core outer surface, can be obtained from equations (2.14) and (2.15). Substituting r=b, p_i=0 and p_o=p into the latter equations, gives

$$\sigma_t = -p(b^2+a^2)/(b^2-a^2),$$

$$\sigma_r = -p.$$

Furthermore, substituting for σ_t and σ_r into equation (2.17) and subsequently into equation (2.16), we will get

$$\Delta = -bp\{(b^2+a^2)/(b^2-a^2) - \mu\}/E, \qquad (2.18)$$

where the minus sign indicates that the deflection is inwards. Equation (2.18) may be rearranged to read,

$$E = -bp\{(1+\alpha^2)/(1-\alpha^2) - \mu\}/\Delta, \qquad (2.19)$$

where, $\alpha = a/b$ = radial ratio, dimensionless. However,

$$-bp/\Delta = p/-\varepsilon_t = E_{eff}, \qquad (2.20)$$

where, E_{eff} = the effective modulus of elasticity of the core material, in Pa or psi.

We can now write, using equations (2.19) and (2.20), a relation expressing the effective elasticity modulus for an isotropic core material, E_{eff}, in terms of only the radial ratio and core material elasticity parameters. The relevant equation is,

$$E_{eff} = \frac{E}{\frac{(1+\alpha^2)}{(1-\alpha^2)} - \mu}, \qquad (2.21)$$

where, μ = Poisson's ratio of the core material, and

E = core material elasticity modulus, in Pa or psi.

(**N.B.** It is not necessary to specify in which direction the material parameters are measured since they are equivalent in all directions for an isotropic material, which is what we are dealing with here.)

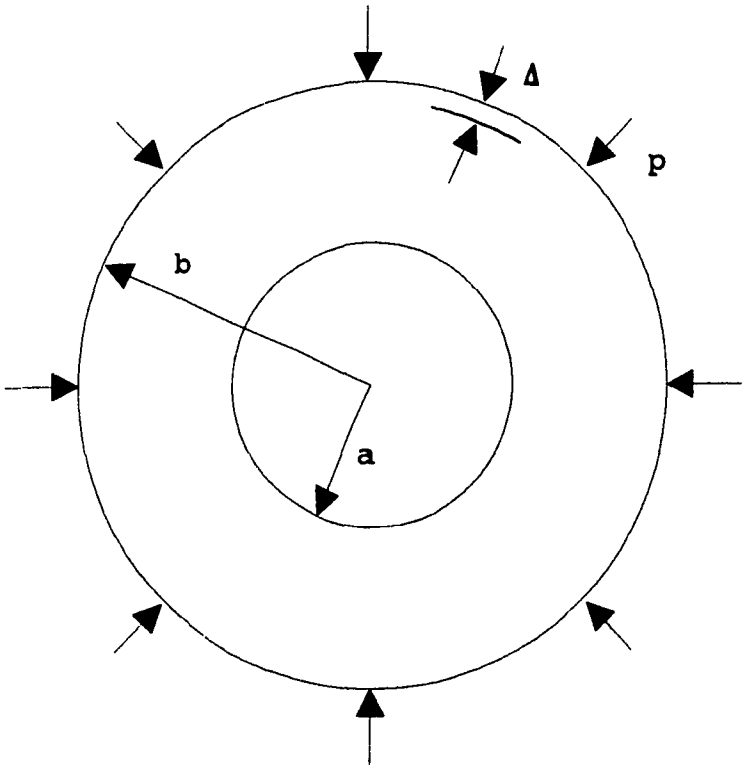

Fig. 2.5: A hollow core.

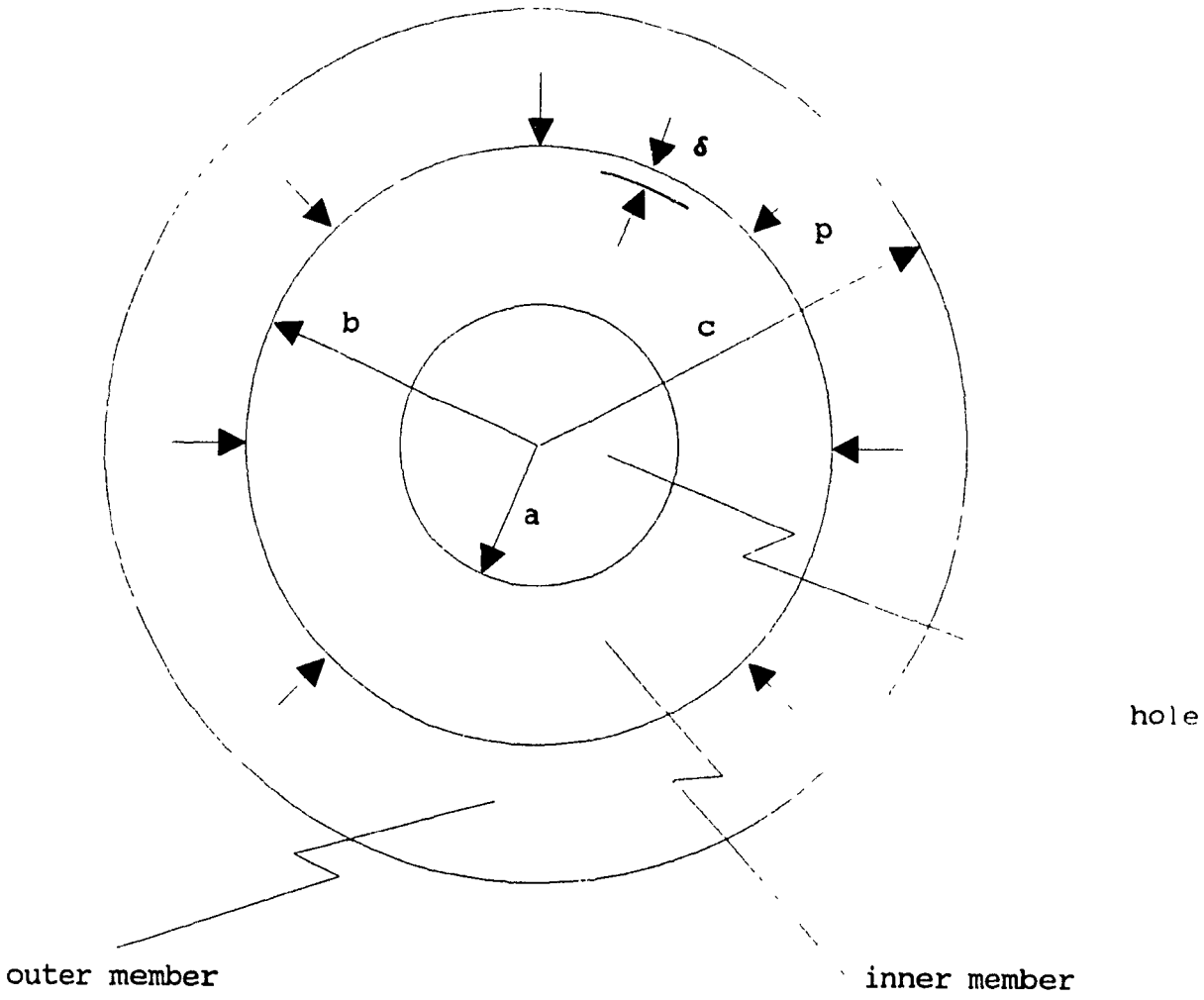

Fig. 2.6: Press-shrink-fit model.

2.3.2 Press-Shrink-Fit Model

The hollow core of Fig. 2.5 may equally be analysed as a press-shrink-fit model (see Fig. 2.6). Referring to the latter figure, the two-element model has three boundaries, the outer and inner radii, and the inside hole radius. Physically, the inside hole and the inner member identically represent a hollow-core situation, whereas the outer member represents the wound roll material surrounding the core. In Fig. 2.6, we designate the hole radius by a, the inner member radius by b, the outer member radius by c; and the pressure developed by the interference fit, which acts uniformly on the interface between the two members, by the symbol p. (**N.B.** External pressure=0, in this case.) Moreover, the radial deformation, at the interface of the boundary b, of the inner member from unloaded to loaded shape using its effective modulus is denoted by the symbol, δ.

Employing the boundary conditions for the inner members at the contact surface, r=b, which are obtained from equations (2.14) and (2.15), respectively; viz.:

$$\sigma_t = -p(b^2+a^2)/(b^2-a^2), \qquad (2.22a)$$

$$\sigma_r = -p; \qquad (2.22b)$$

and applying a similar line of analysis to that of sub-section 2.3.1.2, we have

ε_t = tangential strain in the inner member at radius b,

ε_t = change in circumference/original circumference,

$\varepsilon_t = \{2\pi(b+\delta) - 2\pi b\}/2\pi b$,

$\Rightarrow \quad \varepsilon_t = \delta/b$,

or, $\delta = b\varepsilon_t$.

However, since

$$\varepsilon_t = (\sigma_t/E_i) - (\mu_i\sigma_r/E_i), \tag{2.23}$$

then a relation for δ can be found to read,

$$\delta = -pb\{(b^2+a^2)/(b^2-a^2) - \mu_i\}/E_i, \tag{2.24}$$

where the subscript $(_i)$ denotes quantities associated with the inner member. Continuing with the analysis further, equation (2.24) can be re-written to express the effective core elasticity modulus, E_{eff}, in terms of the radial ratio, α=a/b, and core material properties, E and μ. I.E.,

$$E_{eff} = E/\{(1+\alpha^2)/(1-\alpha^2) - \mu\}, \tag{2.21}$$

where all the notation of equation (2.21) is identical to that of sub-section 2.3.1.2.

It is clearly apparent that the expression for the effective core elasticity modulus (equation (2.21)) obtained through the thick-walled cylinder analysis and the press-shrink-fit model is identical in all respects.

2.3.3 Concluding Remarks Pertaining to The Axisymmetric Model

Equation (2.21), relating the effective core elasticity modulus to the radial ratio and isotropic material parameters of the core material, that is,

$$E_{eff}=\frac{E_t}{\frac{(1+\alpha^2)}{(1-\alpha^2)}-\mu_t}, \tag{2.21}$$

may be re-arranged; if we define a quantity, the modular ratio, denoted by R_e to be the ratio of the effective core elasticity modulus to the core material elasticity modulus in the tangential direction; i.e. $R_e=E_{eff}/E_t$. Equation (2.21) thus becomes,

$$R_e=\frac{1}{\frac{(1+\alpha^2)}{(1-\alpha^2)}-\mu}. \tag{2.25}$$

Equation (2.25) states that as the radial ratio, α, decreases the modular ratio, R_e, increases for a particular isotropic core material. In addition, defining the core thickness ratio, denoted by ß, to be $(1-\alpha)$, then as ß increases the modular ratio, R_e, increases too. In particular, if $\alpha \Rightarrow 1$ (or $ß \Rightarrow 0$), then the modular ratio is expected to approach zero. Conversely, if $\alpha \Rightarrow 0$ ($ß \Rightarrow 1$), corresponding to a situation where we have a solid core; then the modular ratio shoots up. Indeed this statement is physically sound; since the thicker the core material is,

the stiffer it becomes and, vice versa. Figs. 2.7 and 2.8 depict graphically how R_e varies with α and β, respectively. Four materials were examined:

(a) aluminium having the following properties,

$E = 70967$ MPa, and

$\mu = 0.334$;

(b) carbon steel having material properties,

$E = 206700$ MPa, and

$\mu = 0.292$;

(c) same as (a) except for $\mu = 0$; and

(d) same as (b) except for $\mu = 0$.

It is worthy of note that R_e versus α and R_e versus β curves coincide when the Poisson's ratio is equal to zero. Thus indicating that failure to include the Poisson's ratio effect in estimating the effective core material elasticity modulus will ultimately lead to erroneous results. Besides, it is important to note that the Poisson's ratio actually acts to stiffen the core against deflection from external pressure.

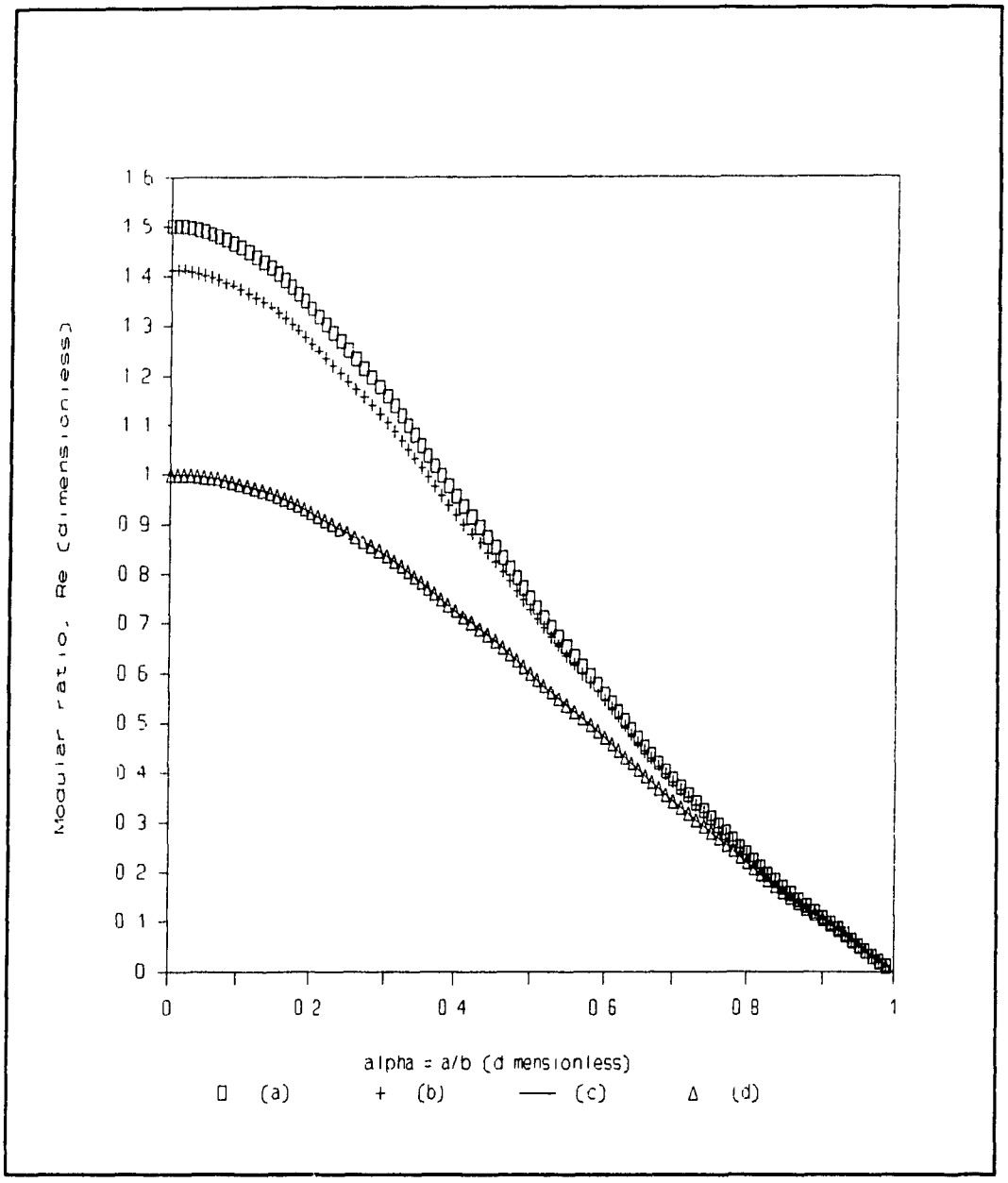

Fig. 2.7: Plots of modular ratio, $R_e=E_{eff}/E$, versus radial ratio, $\alpha=a/b$, for cases (a)-(d) of section 2.3.3 (isotropic condition).

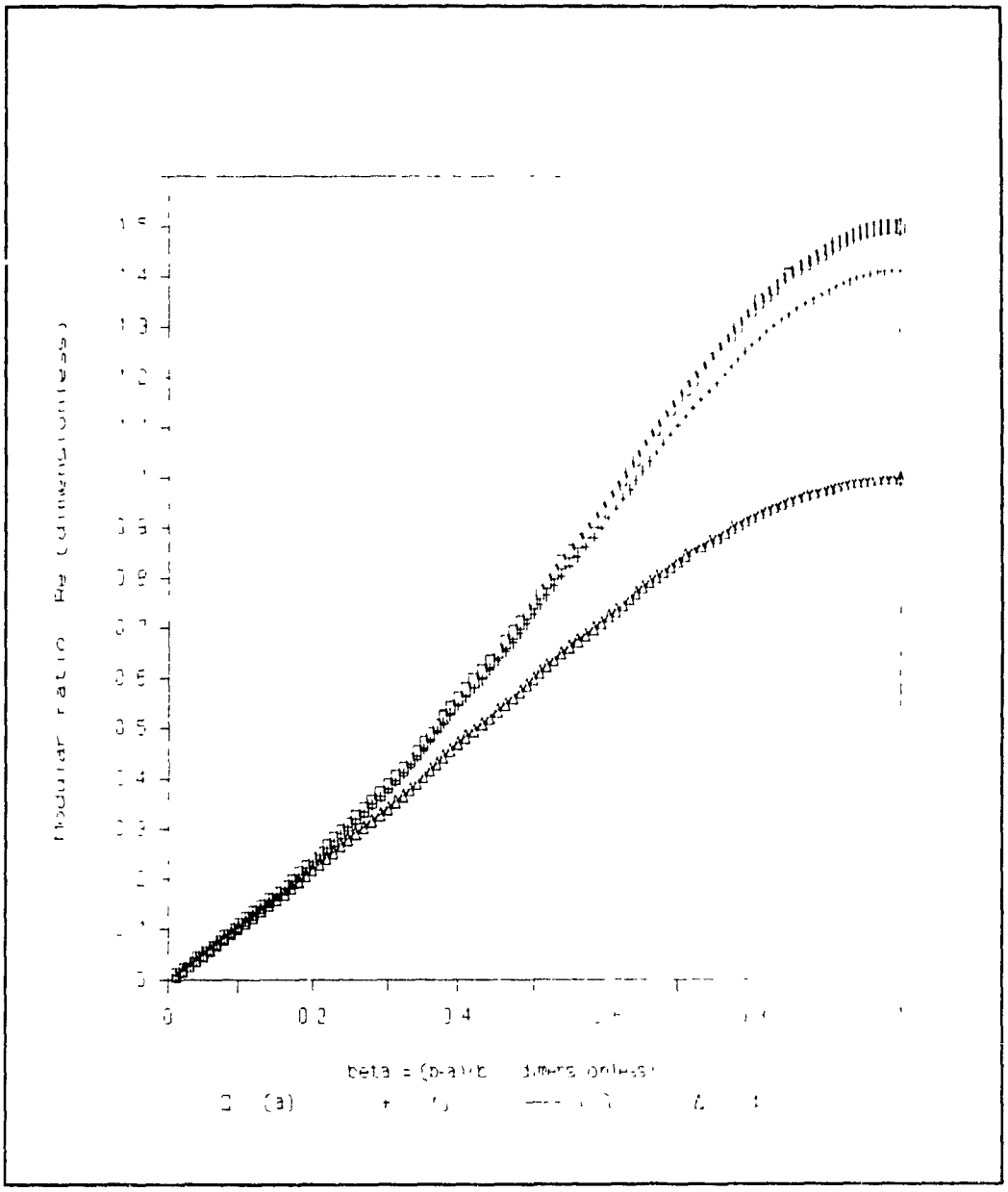

Fig. 2.8: Plots of modular ratio, $R_e=E_{eff}/E$, versus core thickness ratio, $\beta=1-\alpha$, for cases (a)-(d) of section 2.3.3 (isotropic condition).

2.4 FINITE-ELEMENT ANALYSIS OF THE CORE-ROLL SYSTEM

2.4.1 Background

A new investigation is undertaken to find out how the core stiffness affects the roll body at various radii. A finite-element package, I-DEAS^{TM} of Structural Dynamics Corporation running on a Hewlett-Packard 350 workstation, was used to model and analyse the core-roll system. Due to the symmetry of the model under study, only a quarter of the two concentric cylinders representing the core-roll system, need be utilised for analysis. To structurally simulate the actual physical behaviour of the core-roll system, the finite-element model is allowed to freely move horizontally and vertically (see Fig. 2.9), however, the centre of the quarter circle is fixed for all translations and rotations in order to ensure that the structure will not cruise along a particular direction, hence, causing it to be statically unstable. (It is worthwhile noting that negligence to make certain that the static stability condition is satisfied will undoubtedly lead to incorrect results from the finite-element analysis.)

All elements of the finite-element model were analysed as isotropic, thin-shell, quadrilateral or triangular elements where applicable. Three main cases were studied. Below is some detailed account of each one.

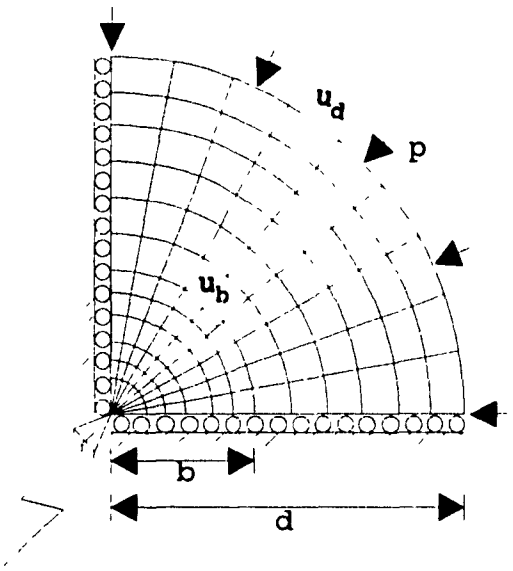

b = core outer radius,

d = roll outer radius,

u_b = radial deformation at b,

u_d = radial deformation at d, and

p = test pressure.

Fig. 2.9: Finite-element model used to find radial deformations at core/roll interface and at roll outer radius under linear isotropic conditions. (Circles indicate frictionless constraint at edges.)

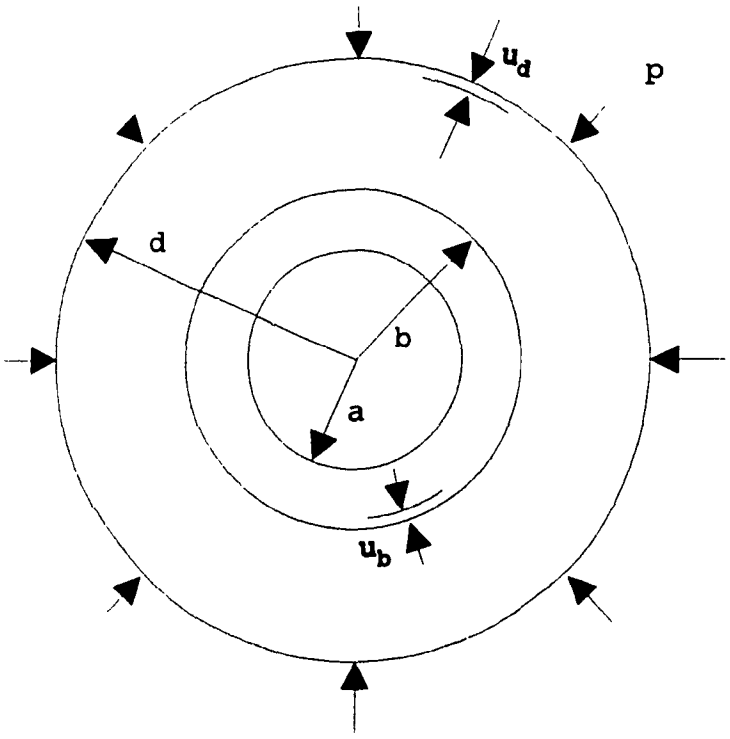

Fig. 2.10: Diagram of core and roll model. Radial deformations u_d and u_b are measured at roll outer radius and core outer radius, respectively. (Radial ratios are: c_1=a/b; and c_2=b/d.)

2.4.2 The Hollow-Core Finite-Element Model

Here, the model consisted of a 1"(2.54 cm)-radius hole surrounded by a core material having the following properties: modulus of elasticity = 30,000,000 psi (206.7 GPa) and, Poisson's ratio = 0.292. (For geometry and finite-element mesh for the hollow-core model see Fig. 2.11.)

The radial deflection at the exterior surface of the core, u_b, was obtained for:

(i) uniform exterior pressure of 100 psi (689 kPa) applied at outer core radius 2.5" (6.35 cm); and

(ii) uniform exterior pressure of 120 psi (826.8 kPa) applied at outer core radius 2.5" (6.35 cm).

The latter case was done so as to examine the effect of increasing the external pressure, that is to say, emulating having more wraps of roll material as in the actual core-roll system; on the radial deflections of the core material at the core exterior surface.

The core radial deflections at the exterior core surface, u_b, obtained from the finite-element analysis are compared with those computed from equation (2.18) or (2.23) previously developed using the thick-walled cylinder analysis and press-shrink-fit model, respectively. Table 2.2 shows details of the numerical results obtained for the aforementioned cases. Examination of Table 2.2 reveals that the u_b values procured analytically and by finite-

element analysis are in good agreement.

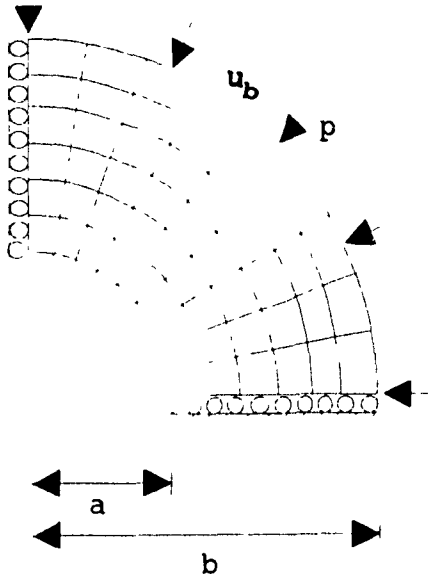

a = core inner radius (hole radius),

b = core outer radius,

u_b = radial deformation at b, and

p = test pressure.

Fig. 2.11: Geometry and finite-element mesh for the hollow-core model.

Table 2.2: Comparison of thick-walled cylinder theory and finite-element analysis results for a hollow core.

Core material parameters:

elasticity modulus = 30,000,000 psi (206 GPa),
Poisson's ratio = 0.292,
hole radius = 1" (2.54 cm).

i. Core outer radius, b = 2.5" (6.35 cm)
Uniform external pressure applied at exterior core surface, p = 100 psi (689 kPa)

* Thick-Walled Cylinder Theory Results

u_b (in)	u_b (cm)	$E_{eff} = p*b/u_b$ (psi)	$E_{eff} = p*b/u_b$ (GPa)
$-9.0746*10^{-6}$	$-2.3049*10^{-5}$	27,549,423.67	189.81

* Finite-Element Analysis

u_b (in)	u_b (cm)	$E_{eff} = p*b/u_b$ (psi)	$E_{eff} = p*b/u_b$ (GPa)
$-9.076*10^{-6}$	$-2.305*10^{-5}$	27,545,174.08	189.79

Table 2.2 Continued.

ii. Core outer radius, b = 2.5" (6.35 cm) Uniform external pressure applied at exterior core surface, p = 120 psi (826.8 kPa)			
* Thick-Walled Cylinder Theory Results			
u_b		$E_{eff} = p*b/u_b$	
(in)	(cm)	(psi)	(GPa)
$-1.0889*10^{-5}$	$-2.7658*10^{-5}$	27,550,739.28	189.82
* Finite-Element Analysis			
u_b		$E_{eff} = p*b/u_b$	
(in)	(cm)	(psi)	(GPa)
$-1.089*10^{-5}$	$-2.766*10^{-5}$	27,548,209.37	189.81

N.B. Minus signs represent inward deflections.

2.4.3 The Solid-Core Finite-Element Model

Fig. 2.12 illustrates the geometry and finite-element mesh generated for the analysis of the solid-core model. Here, the core material had the properties shown below: elasticity modulus = 100,000 psi (689 MPa) and, Poisson's ratio = 0.05. A single run was executed, that for a 2.5" (6.35 cm) solid core to whose exterior surface a uniform external pressure of 100 psi (689 kPa) was applied. Again, the finite-element results for the radial deflections at the core exterior surface were compared with those obtained from equations (2.18) or (2.23); and they were found to be in very good agreement (refer to Table 2.3).

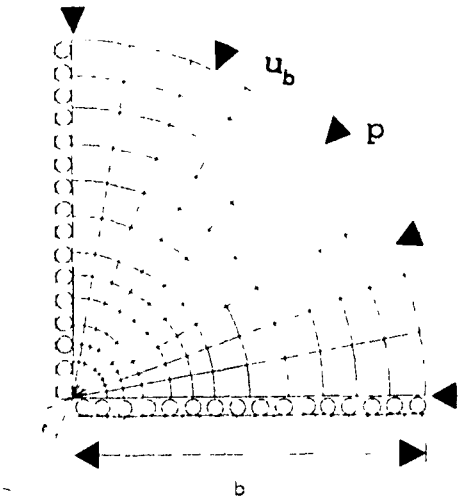

positional restraint

b = core outer radius,

u_b = radial deformation at b,

p = test pressure.

Fig. 2.12: Geometry and finite-element mesh for a solid core model.

Table 2.3: Comparison of thick-walled cylinder theory and finite-element analysis results for a solid core.

Core material parameters:

elasticity modulus = 100,000 psi (689 MPa)

Poisson's ratio = 0.05

Core outer radius, b = 2.5" (6.35 cm) Uniform external pressure applied at exterior core surface, p = 100 psi (689 kPa)			
* Thick-Walled Cylinder Theory Results			
u_b		$E_{eff} = p*b/u_b$	
(in)	(cm)	(psi)	(GPa)
$-2.375*10^{-3}$	$-6.0325*10^{-3}$	105,263.16	725.26
* Finite-Element Analysis			
u_b		$E_{eff} = p*b/u_b$	
(in)	(cm)	(psi)	(GPa)
$-2.375*10^{-3}$	$-6.0325*10^{-3}$	105,263.16	725.26

N.B. Minus signs represent inward deflections.

2.4.4 The Solid Core-Roll Composite Model

This particular investigation was intended to demonstrate how a core of specific material parameters influences the layers of the roll material, being wound around the core, at various radii. The geometry and finite-element mesh generated for this model are shown in Fig. 2.9.

In this model, the core material of radius 1" (2.54 cm) had material parameters as follows: elasticity modulus of 30,000,000 psi (206.7 GPa), and Poisson's ratio of 0.292. Whereas the roll material having the parameters: elasticity modulus = 100,000 psi (689 MPa), and Poisson's ratio = 0.05; was simulated as being wound around the core to outer radii 1.5", 2.5", 3", 3.5" and 4". Each of these outer radii constituted an individual run (the core material properties being the same at all runs) where an exterior uniform pressure, p, of 100 psi (689 MPa) was applied at the exterior surface of the roll. The finite-element model was used to find radial deformations and stresses at the core/roll interface and at the roll outer radius. Radial strains and equivalent roll material moduli at the roll exterior surface could then be computed. The numerical results thus obtained are presented in Table 2.4.

It is evident from the finite-element analysis results that the rate of change of the effective roll modulus with radius is remarkably low. This could be attributed to the

fact that the hardness of the core does not change the hardness of the wound layers that lay on the core as in winding, where the layers of the roll that have been wound on harder substrata are yet harder themselves. This is contrasted by the behaviour of a block of passive material exposed to an external pressure, in which the elasticity modulus of the material does not vary as in the case of winding on bands of web with initial tension due to a winding stress, σ_w, coming in the web.

Therefore, we here conclude our analyses of the various models simulating an isotropic core material, hollow and solid; being part of the core-roll winding system. We shall, thenceforth, direct our attention to investigating anisotropic core materials.

Table 2.4: Finite-element results for a solid core-roll composite model.

Solid core:

core radius, b = 1" (2.54 cm)

elasticity modulus = 30,000,000 psi (206.7 GPa)

Poisson's ratio = 0.292

Roll material:

elasticity modulus = 100,000 psi (689 MPa)

Poisson's ratio = 0.05

Uniform exterior pressure applied at outer roll radius, p = 100 psi (689 kPa)

	Outer Roll Radius, d (in)				
	4	3.5	3	2.5	1.5
u_d (in) ($\times 10^{-3}$)	-3.373	-2.845	-2.303	-1.744	-0.566
$\varepsilon_d = u_d/d$ ($\times 10^{-4}$)	-8.432	-8.128	-7.677	-6.976	-3.773
σ_r (psi)	180.3	177.4	173.2	166.5	135.9
$E_{eff} = pd/u_d$ (psi)	118589	123023	130265	143349	264018

N.B. i) u_d=radial deflection at exterior roll surface,

ii) E_{eff}=effective roll modulus at exterior surface,

iii) σ_r=radial stress at core/roll interface, and

iv) minus signs represent inward deflections.

2.5 THE ANISOTROPIC HOLLOW-CORE MODEL

Thenceforward, we shall introduce to our analysis the fact that the core material exhibits anisotropic behaviour. That is to say, the core material's elastic properties are different for different directions. In particular, we shall model the hollow core as a plate having the shape of a complete circular concentric ring with cylindrical anisotropy. Our ultimate goal is to derive an analytic equation describing the effective elasticity modulus for anisotropic core materials.

In the endeavour to offer a detailed analysis of the anisotropic hollow-core model, we shall first indulge in explaining the definitions, symbolism and theory associated with curvilinear anisotropy and the analysis of a generalised plane stress problem for a body possessing cylindrical anisotropy. This should hopefully provide a clear perception of how the generalised plane stress approach for a body with cylindrical anisotropy can be applied to the hollow-core model. Thereafter, we shall further allow the wound-on material to exhibit anisotropic behaviour, and make deductions thereupon.

2.5.1 Curvilinear Anisotropy

In the study of stresses and deformations in elastic anisotropic bodies, we will consider, on the basis of a generally accepted model [57, 61, 65], that the elastic body is a continuous medium.

A homogeneous anisotropic body, also said to be rectilinearly-anisotropic, is characterised by the equivalence of parallel directions passing through different points of the body. In contrast, however, curvilinear anisotropy is characterised by the fact that in such a body equivalence is not found in parallel directions but follows some other directions. Choosing a system of curvilinear coordinates in such a manner that coordinate directions coincide with equivalent directions at different points of the body, then infinitely small elements of the body, which are delineated by three pairs of coordinate planes, will possess identical elastic properties. Conversely, the elastic properties of elemental rectangular parallelepipeds with mutually parallel sides will not be identical. The number of possible types of curvilinear anisotropy is unlimited. However, we will limit our study to cylindrical anisotropy which indeed reflects the material behaviour of the hollow-core model under investigation.

The axis of anisotropy, which can pass either externally or internally, is represented by a straight

line, g, in the body with cylindrical anisotropy (see Fig. 2.13). All directions which cross this axis at right angles are equivalent. All directions parallel to the anisotropy axis, as well as those orthogonal to the latter are also equivalent. All infinitely small elements A_1, A_2, ... cut from the body by three pairs of surfaces: (a) two planes passing through the axis of anisotropy; (b) two parallel planes normal to g and (c) two concentric cylindrical surfaces with the axis which coincides with g (Fig. 2.13); all such elements have identical elastic properties.

It would be prudent as well as convenient to use cylindrical coordinates; r, θ, z, during our analysis of the problem at hand, with the z-axis coinciding with the axis of anisotropy, g, and with an arbitrarily chosen polar axis, x, from which angle θ is measured.

The equations of the generalised Hooke's law for a body with cylindrical anisotropy of the general type without any elastic symmetry are:

$$
\begin{aligned}
\varepsilon_r &= a_{11}\sigma_r+a_{12}\sigma_\theta+a_{13}\sigma_z+a_{14}\tau_{\theta z}+a_{15}\tau_{rz}+a_{16}\tau_{r\theta},\\
\varepsilon_\theta &= a_{12}\sigma_r+a_{22}\sigma_\theta+ \ldots\ldots\ldots\ldots\ldots +a_{26}\tau_{r\theta},\\
\varepsilon_z &= a_{13}\sigma_r+a_{23}\sigma_\theta+ \ldots\ldots\ldots\ldots\ldots +a_{36}\tau_{r\theta},\\
\gamma_{\theta z} &= a_{14}\sigma_r+a_{24}\sigma_\theta+ \ldots\ldots\ldots\ldots\ldots +a_{46}\tau_{r\theta},\\
\gamma_{rz} &= a_{15}\sigma_r+a_{25}\sigma_\theta+ \ldots\ldots\ldots\ldots\ldots +a_{56}\tau_{r\theta},\\
\gamma_{r\theta} &= a_{16}\sigma_r+a_{26}\sigma_\theta+ \ldots\ldots\ldots\ldots\ldots +a_{66}\tau_{r\theta}.
\end{aligned}
\qquad (2.26)
$$

In equations (2.26), ε_r, ε_θ, ... $\gamma_{r\theta}$ are the components of deformation; σ_r, σ_θ, ... $\tau_{r\theta}$ are the stress components on planes normal to coordinates r, θ, z of the cylindrical system, and the coefficients a_{ij} designate the elasticity constants (which are usually expressed in terms of elasticity parameters) [57, 65].

Above, we have adopted the commonly used notation to designate each normal stress component by σ with a subscript indicating the direction of the normal to the plane, and consequently, the direction of the component itself. Further, each tangential component is designated by τ with two subscripts, the first one indicating the direction of the component, and the other, the direction of the normal to the plane. As for the components of deformation, ε is used, with the appropriate subscript, to designate relative elongations for the directions r, θ, z; and γ, with two subscripts, to designate three relative shears. The number of independent constants in equations (2.26), in general, is 21. Different types of elastic symmetry are possible for a body with cylindrical anisotropy; which will consequently lead to reducing the number of independent constants in equations (2.26).

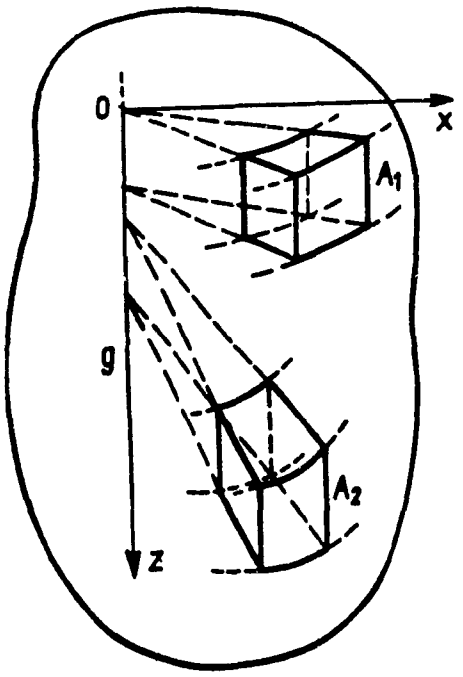

Fig. 2.13: Elements of a body with cylindrical anisotropy. The axis of anisotropy is designated by g, and A_1 and A_2 represent elements of the body [65].

2.5.2 Generalised Plane Stress For a Body Possessing Cylindrical Anisotropy

In this sub-section, we will consider the equilibrium of a thin prismatic body, a plate, which has a constant thickness in the z-direction (see Fig. 2.14) and possesses cylindrical anisotropy; as a result of forces distributed along the edges and, of body forces. The following, with respect to elastic properties, will be assumed:

1. the axis of anisotropy, g, is normal to the middle plane of the plate (the intersection of the axis of anisotropy with the middle plane, which is frequently referred to as the pole of anisotropy, may be located inside, outside or on the edge of the plate), and
2. each point has a plane of elastic symmetry which is normal to the axis of anisotropy (and, consequently, is parallel to the middle plane).

Furthermore, it will be assumed that the surface and body forces are parallel to the middle plane, as well as distributed symmetrically relative to this plane and vary only slightly with respect to the thickness. The deformation will be considered to be small.

Referring to Fig. 2.14, we have chosen the axis of anisotropy to be the z-axis of the system of cylindrical coordinates r, θ, z and, the direction of the polar x-axis is arbitrary within the middle plane. We shall denote the plate thickness by h, and the body forces per unit volume

in coordinate directions r, Θ, z by **R**, **T**, **Z**, respectively. It is worthy of note to recognise that **Z**=0 for our plate; since the faces of the plate are entirely free from applied loads (a necessary assumption for the generalised plane stress situation). In studying the state of plane stress it is advantageous, because of the basic assumptions, to introduce the average values with respect to thickness of the stress components and displacements: σ_r^*, σ_Θ^*, σ_z^*, $\tau_{r\Theta}^*$, u_r^*, u_Θ^*. These values are designated as integrals of corresponding stresses and displacements taken over the thickness and divided by it; i.e.,

$$\sigma_r^* = \frac{1}{h}\int_{-\frac{h}{2}}^{\frac{h}{2}} \sigma_r dz,$$

$$\sigma_\theta^* = \frac{1}{h}\int_{-\frac{h}{2}}^{\frac{h}{2}} \sigma_\theta dz,$$

$$\sigma_z^* = \frac{1}{h}\int_{-\frac{h}{2}}^{\frac{h}{2}} \sigma_z dz,$$

$$\tau_{r\theta}^* = \frac{1}{h}\int_{-\frac{h}{2}}^{\frac{h}{2}} \tau_{r\theta} dz, \qquad (2.27)$$

$$u_r^* = \frac{1}{h}\int_{-\frac{h}{2}}^{\frac{h}{2}} u_r dz, \text{ and } u_\theta^* = \frac{1}{h}\int_{-\frac{h}{2}}^{\frac{h}{2}} u_\theta dz.$$

Moreover, we will also introduce the notation:

$$\boldsymbol{R}^{*}=\frac{1}{h}\int_{-\frac{h}{2}}^{\frac{h}{2}}\boldsymbol{R}dz,\ \textit{and}\ \boldsymbol{T}^{*}=\frac{1}{h}\int_{-\frac{h}{2}}^{\frac{h}{2}}\boldsymbol{T}dz, \tag{2.28}$$

where $\mathbf{R}^{*}$ and $\mathbf{T}^{*}$ are the average values of body forces with respect to the thickness. It is assumed that the body forces are derivable from a potential $U(r,\theta)$, i.e., they are determined from formulae

$$\mathbf{R}^{*} = -\partial U^{*}/\partial r,$$

$$\mathbf{T}^{*} = -(1/r)(\partial U^{*}/\partial \theta), \tag{2.29}$$

where U^{*} designates the averaged (with respect to thickness) potential.

Similarly, we can obtain the average values, with respect to thickness, of the components of deformation; ε_r^{*}, ε_Θ^{*}, $\gamma_{r\Theta}^{*}$, which, assuming small deformations, are equal to:

$$\varepsilon_r^{*} = \partial u_r^{*}/\partial r,$$

$$\varepsilon_\Theta^{*} = (1/r)(\partial u_\Theta^{*}/\partial \theta) + (u_r^{*}/r), \tag{2.30}$$

$$\gamma_{r\Theta}^{*} = (1/r)(\partial u_r^{*}/\partial \theta) + (\partial u_\Theta^{*}/\partial r) - (u_\Theta^{*}/r).$$

(**N.B.** Equations (2.30) are true for any continuous body, both elastic and inelastic. Derivations of these equations can be found in textbooks on the theory of elasticity, eg. [57, 67, 68].)

The equilibrium equations in cylindrical coordinates

read,

$$(\partial\sigma_r/\partial r)+(1/r)(\partial\tau_{r\theta}/\partial\theta)+(\partial\tau_{rz}/\partial z)+((\sigma_r-\sigma_\theta)/r)+R = 0,$$

$$(\partial\tau_{r\theta}/\partial r)+(1/r)(\partial\sigma_\theta/\partial\theta)+(\partial\tau_{\theta z}/\partial z)+(2\tau_{r\theta}/r)+T = 0, \qquad (2.31)$$

$$(\partial\tau_{rz}/\partial r)+(1/r)(\partial\tau_{\theta z}/\partial\theta)+(\partial\sigma_z/\partial z)+(\tau_{rz}/r)+Z = 0.$$

And the equations of the generalised Hooke's law (2.26) in which, since we have a case of one plane of elastic symmetry; the number of independent elastic constants reduces to 13 because,

$a_{14}=a_{15}=a_{24}=a_{25}=a_{34}=a_{35}=a_{46}=a_{56}=0$, and thence equations (2.26) become,

$$\begin{aligned}
\varepsilon_r &= a_{11}\sigma_r+a_{12}\sigma_\theta+a_{13}\sigma_z+a_{16}\tau_{r\theta},\\
\varepsilon_\theta &= a_{12}\sigma_r+a_{22}\sigma_\theta+a_{23}\sigma_z+a_{26}\tau_{r\theta},\\
\varepsilon_z &= a_{13}\sigma_r+a_{23}\sigma_\theta+a_{33}\sigma_z+a_{36}\tau_{r\theta}, \qquad (2.32)\\
\gamma_{\theta z} &= a_{11}\tau_{\theta z}+a_{45}\tau_{rz},\\
\gamma_{rz} &= a_{45}\tau_{\theta z}+a_{55}\tau_{rz}, \text{ and}\\
\gamma_{r\theta} &= a_{16}\sigma_r+a_{26}\sigma_\theta+a_{36}\sigma_z+a_{66}\tau_{r\theta}.
\end{aligned}$$

By averaging (i.e. by multiplying by dx/h and integrating over the thickness) equations (2.31) and (2.32); and disregarding σ_z^*, since it is negligible compared with σ_r^*, σ_θ^* and $\tau_{r\theta}^*$, we obtain <u>five equilibrium equations</u>, which correspond to the number of unknown functions; namely,

$$(\partial\sigma_r^*/\partial r)+(1/r)(\partial\tau_{r\theta}^*/\partial\theta)+((\sigma_r^*-\sigma_\theta^*)/r)+R^* = 0,$$

$$(\partial\tau_{r\theta}^*/\partial r)+(1/r)(\partial\sigma_\theta^*/\partial\theta)+(2\tau_{r\theta}^*/r)+T^* = 0; \qquad (2.33)$$

$$\begin{aligned}
\varepsilon_r^* &= a_{11}\sigma_r^*+a_{12}\sigma_\theta^*+a_{16}\tau_{r\theta}^*,\\
\varepsilon_\theta^* &= a_{12}\sigma_r^*+a_{22}\sigma_\theta^*+a_{26}\tau_{r\theta}^*, \qquad (2.34)\\
\gamma_{r\theta}^* &= a_{16}\sigma_r^*+a_{26}\sigma_\theta^*+a_{66}\tau_{r\theta}^*.
\end{aligned}$$

The equation of compatibility may be obtained by eliminating the displacements from equations (2.30); namely:

$$(\partial^2\varepsilon_r^*/\partial\theta^2)+r(\partial^2(r\varepsilon_\theta^*)/\partial r^2)-(\partial^2(r\gamma_{r\theta}^*)/\partial r\partial\theta)-$$
$$r(\partial\varepsilon_r^*/\partial r) = 0. \qquad (2.35)$$

The equilibrium equations (2.33) are identically satisfied by the introduction of a stress function $F(r,\theta)$ and if we set:

$$\begin{aligned}\sigma_r^* &= (1/r)(\partial F/\partial r)+(1/r^2)(\partial^2F/\partial\theta^2)+U^*,\\ \sigma_\theta^* &= (\partial^2F/\partial r^2)+U^*, \qquad (2.36)\\ \tau_{r\theta}^* &= -\partial^2(F/r)/\partial r\partial\theta,\end{aligned}$$

where U^* is the (averaged) potential previously encountered in equations (2.29). On the basis of the compatibility equation (2.35), equilibrium equations (2.34) and (2.36); we obtain the differential equation which must be satisfied by the stress function:

$$\begin{aligned}&a_{22}(\partial^4F/\partial r^4)-2a_{26}(1/r)(\partial^4F/\partial r^3\partial\theta)+\\ &(2a_{12}+a_{66})(1/r^2)(\partial^4F/\partial r^2\partial\theta^2)-2a_{16}(1/r^3)(\partial^4F/\partial r\partial\theta^3)+\\ &a_{11}(1/r^4)(\partial^4F/\partial\theta^4)+2a_{22}(1/r)(\partial^3F/\partial r^3)-\\ &(2a_{12}+a_{66})(1/r^3)(\partial^3F/\partial r\partial\theta^2)+2a_{16}(1/r^4)(\partial^3F/\partial\theta^3)-\\ &a_{11}(1/r^2)(\partial^2F/\partial r^2)-2(a_{16}+a_{26})(1/r^3)(\partial^2F/\partial r\partial\theta)+\\ &(2a_{11}+2a_{12}+a_{66})(1/r^4)(\partial^2F/\partial\theta^2)+a_{11}(1/r^3)(\partial F/\partial r)+\\ &2(a_{16}+a_{26})(1/r^4)(\partial F/\partial\theta) = -(a_{12}+a_{22})(\partial^2U^*/\partial r^2)+\\ &(a_{16}+a_{26})(1/r)(\partial^2U^*/\partial r\partial\theta)-(a_{11}-a_{12})(1/r^2)(\partial^2U^*/\partial\theta^2)+\\ &(a_{11}-2a_{22}-a_{12})(1/r)(\partial U^*/\partial r)+(a_{16}+a_{26})(1/r^2)(\partial U^*/\partial\theta).\end{aligned}$$
$$\ldots\ldots\ldots \qquad (2.37)$$

Due to the considerable complexity of equation (2.37), principally, since it contains the derivatives of the stress function F of different orders, from the first to the fourth; a general expression for F in terms of arbitrary functions is excruciatingly difficult to find. To the author's best knowledge, general expressions for F have only been found using the theory of complex variables, for much simpler cases where the differential equation does not involve different orders of the derivatives of F, as in the cases of isotropic or orthotropic materials [64, 65, 67].

In particular, if the plate with cylindrical anisotropy is at the same time also orthotropic, i.e., has three planes of elastic symmetry at each point, of which one is parallel to the middle plane, the second passes through the axis of anisotropy, and the third is orthogonal to the first two, then equations (2.34) can be written (**N.B.** $a_{16}=a_{26}=a_{36}=a_{46}=0$):

$$\begin{aligned} \varepsilon_r^* &= (1/E_r)\sigma_r^* - (\mu_\Theta/E_\Theta)\sigma_\Theta^*, \\ \varepsilon_\Theta^* &= -(\mu_r/E_r)\sigma_r^* + (1/E_\Theta)\sigma_\Theta^*, \\ \gamma_{r\Theta}^* &= (1/G_{r\Theta})\tau_{r\Theta}^*, \end{aligned} \qquad (2.34a)$$

here E_r, E_Θ are Young's moduli for tension (compression) along principal directions r and Θ; μ_r, μ_Θ are Poisson's ratio in the radial and tangential directions, respectively; and $G_{r\Theta}$ the shear modulus which characterises the change of angles between principal directions r and θ.

The differential equation which must be satisfied by the stress function, equation (2.37), for this case is simplified to

$$(1/E_\Theta)(\partial^4F/\partial r^4) + [(1/G_{r\Theta})-(2\mu_r/E_r)](1/r^2)(\partial^4F/\partial r^2\partial\theta^2) + (1/E_r)(1/r^4)(\partial^4F/\partial\theta^4) + (2/E_\Theta)(1/r)(\partial^3F/\partial r^3) - [(1/G_{r\Theta})-(2\mu_r/E_r)](1/r^3)(\partial^2F/\partial r\partial\theta^2) - (1/E_r)(1/r^2)(\partial^2F/\partial r^2) + \{[2(1-\mu_r)/E_r]+(1/G_{r\Theta})\}(1/r^4)(\partial^2F/\partial\theta^2) + (1/E_r)(1/r^3)(\partial F/\partial r) = -[(1-\mu_\Theta)/E_\Theta](\partial^2U^*/\partial^2) - [(1-\mu_r)/E_r](1/r^2)(\partial^2U^*/\partial\theta^2) - \{(2/E_\Theta)-[(1+\mu_r)/E_r]\}(1/r)(\partial U^*/\partial r). \quad \ldots\ldots\ldots\ldots\ldots \quad (2.37a)$$

The boundary conditions for given forces at the plate edge can be expressed in terms of the first derivatives of the stress function $(\partial F/\partial r)$ and $(\partial F/\partial\theta)$ at the contour of the region occupied by the plate.

Moreover, by superimposing the directions of axes x and y on the principal directions of elasticity for an orthotropic plate (see Fig. 2.14), and in the absence of body forces; the following homogeneous equation is obtained instead of equation (2.37) [70]:

$$(1/E_2)(\partial^4F/\partial x^4) + [(1/G)-(2\mu_1/E_1)](\partial^4F/\partial x^2\partial y^2) + (1/E_1)(\partial^4F/\partial y^4) = 0, \quad \ldots\ldots \quad (2.37b)$$

where E_1, E_2 are the Young's moduli for tension (compression) along the principal directions x and y; $G=G_{12}$, the shear modulus which characterises the change of angles

between principal directions x and y; and $\mu_1=\mu_{12}$ the Poisson's ratio which characterises the dimensional decrease in direction y during tension in direction x.

However, in the case of an isotropic plate in which material parameters are equivalent in all directions; i.e. $E_1=E_2=E$, and $G=E/2(1+\mu)$, then equation (2.37b) becomes the biharmonic equation [71]. I.E.,

$$\nabla^2\nabla^2 F=0, \qquad (2.37c)$$

where ∇^2 is the two-dimensional Laplacian operator:

$$\nabla^2 = (\partial^2/\partial x^2) + (\partial^2/\partial y^2).$$

Expanded, equation (2.37c) is written as:

$$(\partial^4 F/\partial x^4) + 2(\partial^4 F/\partial x^2\partial y^2) + (\partial^4 F/\partial y^4) = 0. \qquad (2.37c')$$

We shall henceforth direct our attention to determining the stress distribution in an annular plate with cylindrical anisotropy which ultimately leads to solving the anisotropic hollow-core problem.

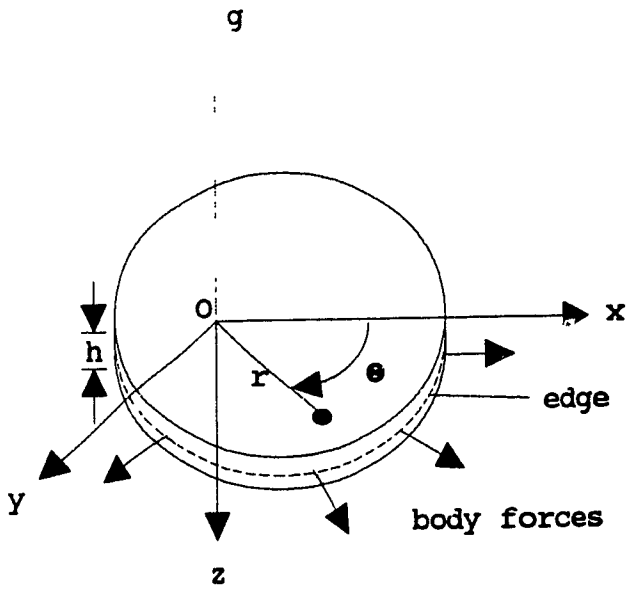

Fig. 2.14: General situation where generalised plane stress is applicable.

2.5.3 Stress Distribution in an Annular Plate with Cylindrical Anisotropy

As has already been stated, the hollow core made up of anisotropic material was modelled as an annular plate, of certain thickness, h, with cylindrical anisotropy. The findings of sub-section 2.5.2 for analysing a body possessing cylindrical anisotropy, in a (generalised) plane stress situation, will now be applied to determining the stress distribution of a plate having the shape of a complete circular concentric ring with cylindrical anisotropy and compressed along the external and internal surfaces by a uniformly distributed normal load (see Fig. 2.15). In considering the elastic equilibrium of the plate, the anisotropy pole will be taken to coincide with the ring centre. It will further be considered that there are no elements of elastic symmetry besides the planes which are parallel to the middle plane. By solving this problem, we obtain at the same time the solution to the analogous problem regarding the stress distribution in a (hollow) core made up of material with cylindrical anisotropy subjected to external and/or internal pressures.

By having the anisotropy pole (the ring centre) as the origin of coordinates, the polar x-axis may be directed arbitrarily (see Fig. 2.15). In reference to the same figure, we designate the magnitudes of the internal and external pressures per unit area by p and q, respectively,

the internal and external plate radii by a and b, and the radius to a point inside the plate by r. Assuming that $U^*=0$ and using a stress function F, independent of polar angle θ (since the plate is axisymmetric), which reads

$$F = A + Br^2 + Cr^{1+k} + Dr^{1-k}, \tag{2.38}$$

where A, B, C and D are constants (to be determined from the boundary conditions) and,

$$k = \text{anisotropy ratio},$$
$$= (a_{11}/a_{22})^{\frac{1}{2}} = (E_\theta/E_r)^{\frac{1}{2}}. \tag{2.39}$$

E_r and E_θ are Young's moduli for tension (or compression) in the radial and tangential directions r and θ, respectively. Upon so doing, the stress components (averaged relative to thickness) are expressed by stress function F, of formulae (2.36), where $U^*=0$. Function F satisfies equation (2.37), where again $U^*=0$. We are now able to determine the stress components, σ_r, σ_θ, $\tau_{r\theta}$. They are:

$$\sigma_r=\frac{(pc^{k+1}-q)}{(1-c^{2k})}\left(\frac{r}{b}\right)^{k-1}-\frac{(p-qc^{k-1})}{(1-c^{2k})}c^{k+1}\left(\frac{b}{r}\right)^{k+1},$$

$$\sigma_\theta=\frac{(pc^{k+1}-q)}{(1-c^{2k})}k\left(\frac{r}{b}\right)^{k-1}+\frac{(p-qc^{k-1})}{(1-c^{2k})}kc^{k+1}\left(\frac{b}{r}\right)^{k+1}, \tag{2.40}$$

$$\tau_{r\theta}=0,$$

where, c = a/b = radial ratio.

It is worthwhile mentioning that the stress distribution, indicated by equations (2.40), is identical for all radial cross sections and depends only on the ratio of Young's moduli for tension (compression) in the tangential and radial directions.

Displacements of points in the plate in the radial and tangential directions u_r and u_θ can, hence, be found from the generalised Hooke's law equations (2.32) for the case of one plane of elastic symmetry. They are:

$$u_r = \frac{b}{E_\theta(1-c^{2k})}\left[(pc^{k+1}-q)(k-\mu_\theta)\left(\frac{r}{b}\right)^k + (p-qc^{k-1})c^{k+1}(k+\mu_\theta)\left(\frac{b}{r}\right)^k\right]$$

$$u_\theta = 0, \tag{2.41}$$

where E_θ and μ_θ are Young's elasticity modulus and Poisson's ratio, respectively, for principal directions, θ.

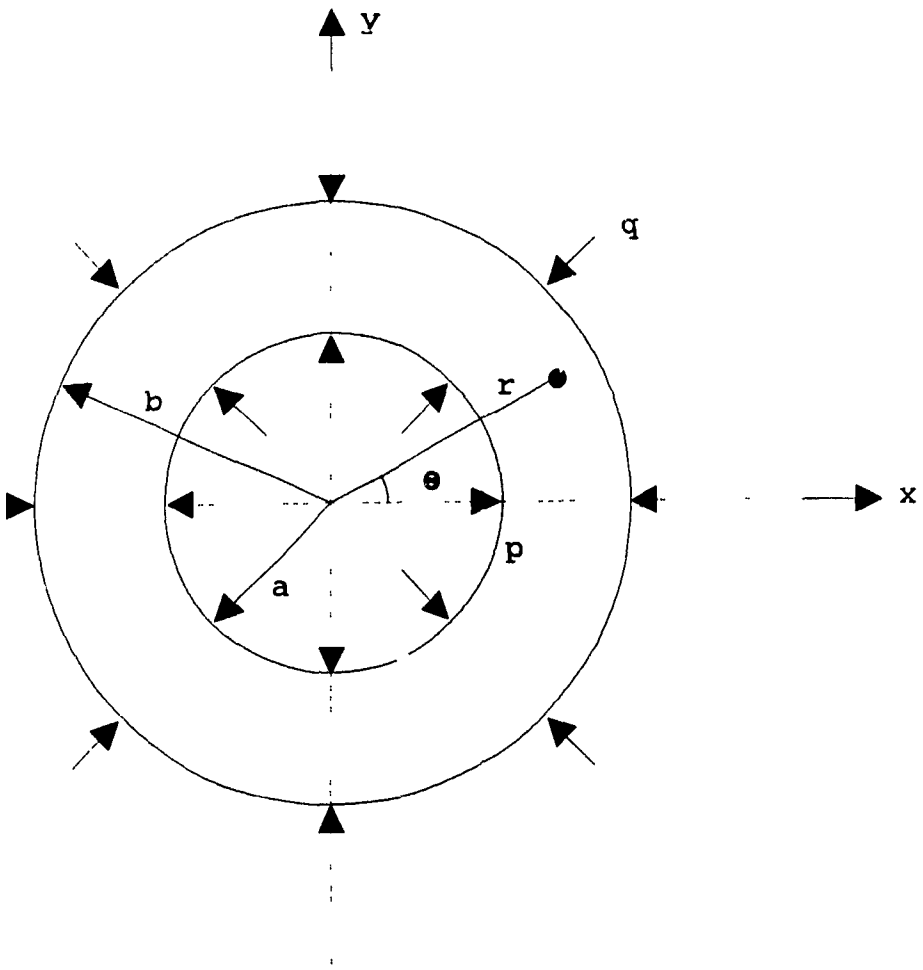

Fig. 2.15: Diagram illustrating a cross-section of an annular plate with cylindrical anisotropy. The internal and external pressures are denoted by p and q, whilst a and b are used to designate the inner and outer radii of the plate. θ is the polar angle and r represents the radius to any point inside the plate.

2.5.4 Interpretations & Conclusions

2.5.4.1 The Hollow-Core Problem: Anisotropic and Isotropic Materials

The theory and analysis of an annular plate with cylindrical anisotropy can now be easily used to derive an analytic expression for the effective elasticity modulus of an anisotropic hollow core under the influence of only external pressure, caused by the wraps of roll material wound around the core. Adopting the same notation previously implemented (refer to Fig. 2.15), i.e., q to denote uniform pressure at the exterior core surface (the internal pressure being zero) and, a and b to denote the inner and outer core radii; the radial deflection at the core's exterior surface (at r=b), u_r, can now be obtained from equation (2.41) as

$$u_r=-qb\frac{[(k-\mu_\theta)+c^{2k}(k+\mu_\theta)]}{E_\theta(1-c^{2k})}=-\frac{qb}{E_\theta}\left[\frac{k(1+c^{2k})}{(1-c^{2k})}-\mu_\theta\right], \qquad (2.42)$$

where the minus sign signifies that the core radial deflection is inwards, as expected. Dividing equation (2.42) by b, inverting the resulting equation and, finally, multiplying by q; will give an expression for the effective core elasticity modulus, E_{eff}, (note that $E_{eff}=qb/-u_r$) in terms of the tangential Young's modulus, E_Θ, radial ratio, c, tangential Poisson's ratio, μ_Θ; and the material anisotropy ratio, k, defined by relation (2.39). This

expression reads,

$$E_{eff}=\frac{E_\theta(1-c^{2k})}{(k-\mu_\theta)+c^{2k}(k+\mu_\theta)}=\frac{E_\theta}{\frac{k(1+c^{2k})}{(1-c^{2k})}-\mu_\theta}. \qquad (2.43a)$$

It is worthy of note, at this stage, that the assumption of zero pressure on the interior of the core presumes that the interior wall is unsupported by any other rigid body. If there is contact with a stiff inside cylinder, then the determination of the exterior deflection becomes more complex. Furthermore, the effective core modulus can be found from equation (2.43a) provided that E_Θ and E_r can be evaluated; which may not always be an easy task, particularly in the case of fibre tube cores [26].

Defining the modular ratio, R_e, to be the ratio of effective core elasticity modulus to tangential elasticity modulus, i.e. $R_e=E_{eff}/E_\Theta$, then equation (2.43a) becomes

$$R_e=\frac{E_{eff}}{E_\theta}=\frac{1}{\frac{k(1+c^{2k})}{(1-c^{2k})}-\mu_\theta} \qquad (2.43b)$$

This relationship is graphed against the radial ratio, c=a/b, for linear anisotropic materials with Poisson's ratio of 0.1 and k values of 2, 4 and 8 (Fig. 2.16). The highest value of k might be taken as appropriate for a model for spiral-wound-paper-tube cores where E_Θ is on the order of 600,000 psi (4.2 MPa), however this material is known to be non-linear in compression, so k will be a

function of pressure [9]. Ostensibly, for linear isotropic materials (i.e. k=1) such as aluminium or carbon steel, equation (2.43b) reduces to equation (2.25) previously encountered in sub-section (2.3.3). Fig. 2.17 which graphically illustrates relationship (2.43b) for linear isotropic materials, using Poisson's ratio of zero and 0.334; shows that Poisson's ratio acts to stiffen the core against deflection from external pressure. Here the elasticity modulus is increased by roughly 50% when Poisson's ratio goes from 0 to 0.334. Additional strains are produced in the tangential and axial directions when there is a constant Poisson's ratio. These strains are proportional to the radial strain caused by external pressure. The net effect is to reduce the radial deformation, which results in a higher effective modulus.

The rate of change of effective core elasticity modulus with radial ratio, for anisotropic core materials with tangential elasticity modulus, $E_\Theta = k^2 \times E_r$; is greatly reduced as can be surmised from Fig. 2.16. When the radial modulus is low compared to the tangential modulus, a small amount of radial deformation will cause inward strains that produce like amounts of tangential strain. In the presence of a high tangential modulus, these strains will cause large tangential stresses, thus causing the core tube to act as props to support the external pressure so it does not penetrate deeply into the underlying layers. In Fig.

2.16 at radial ratio, a/b=0.80 (wall thickness 20% of the outer radius), little if any increase in modulus occurs if the wall thickness is increased to 35% (i.e. a/b=0.65). This shows that it does not pay to add material to the inside of the core because little of the external load is carried on to the inner layers.

Equations (2.40), previously derived in sub-section 2.5.3, predict the distribution of radial and tangential stresses inside a core as a function only of geometry, anisotropy ratio, k, and the internal and external pressures; namely,

$$\sigma_r = \frac{(pc^{k+1}-q)}{(1-c^{2k})}\left(\frac{r}{b}\right)^{k-1} - \frac{(p-qc^{k-1})}{(1-c^{2k})}c^{k+1}\left(\frac{b}{r}\right)^{k+1},$$

$$\sigma_\theta = \frac{(pc^{k+1}-q)}{(1-c^{2k})}k\left(\frac{r}{b}\right)^{k-1} + \frac{(p-qc^{k-1})}{(1-c^{2k})}kc^{k+1}\left(\frac{b}{r}\right)^{k+1}, \qquad (2.40)$$

$$\tau_{r\theta} = 0.$$

It is interesting to note that these equations do not include Poisson's ratio. In the particular case of isotropic materials, when k=1, equations (2.40) reduce to the known Lamé equations [72]:

$$\sigma_r = \frac{(pc^2-q)}{(1-c^2)} - \frac{(p-q)}{(1-c^2)}c^2\left(\frac{b}{r}\right)^2, \qquad (2.44)$$

$$\sigma_\theta = \frac{(pc^2-q)}{(1-c^2)} + \frac{(p-q)}{(1-c^2)}c^2\left(\frac{b}{r}\right)^2, \text{ and } \tau_{r\theta} = 0,$$

where all symbols are as defined earlier. The above equations are identical to the general expressions for the radial and tangential stresses (equations (2.14) and (2.15)) obtained from the thick-walled cylinder theory. The stresses within an isotropic hollow core then vary as a function of $(1/r^2)$, as in the case of a hollow shaft over which a hub is press-fit.

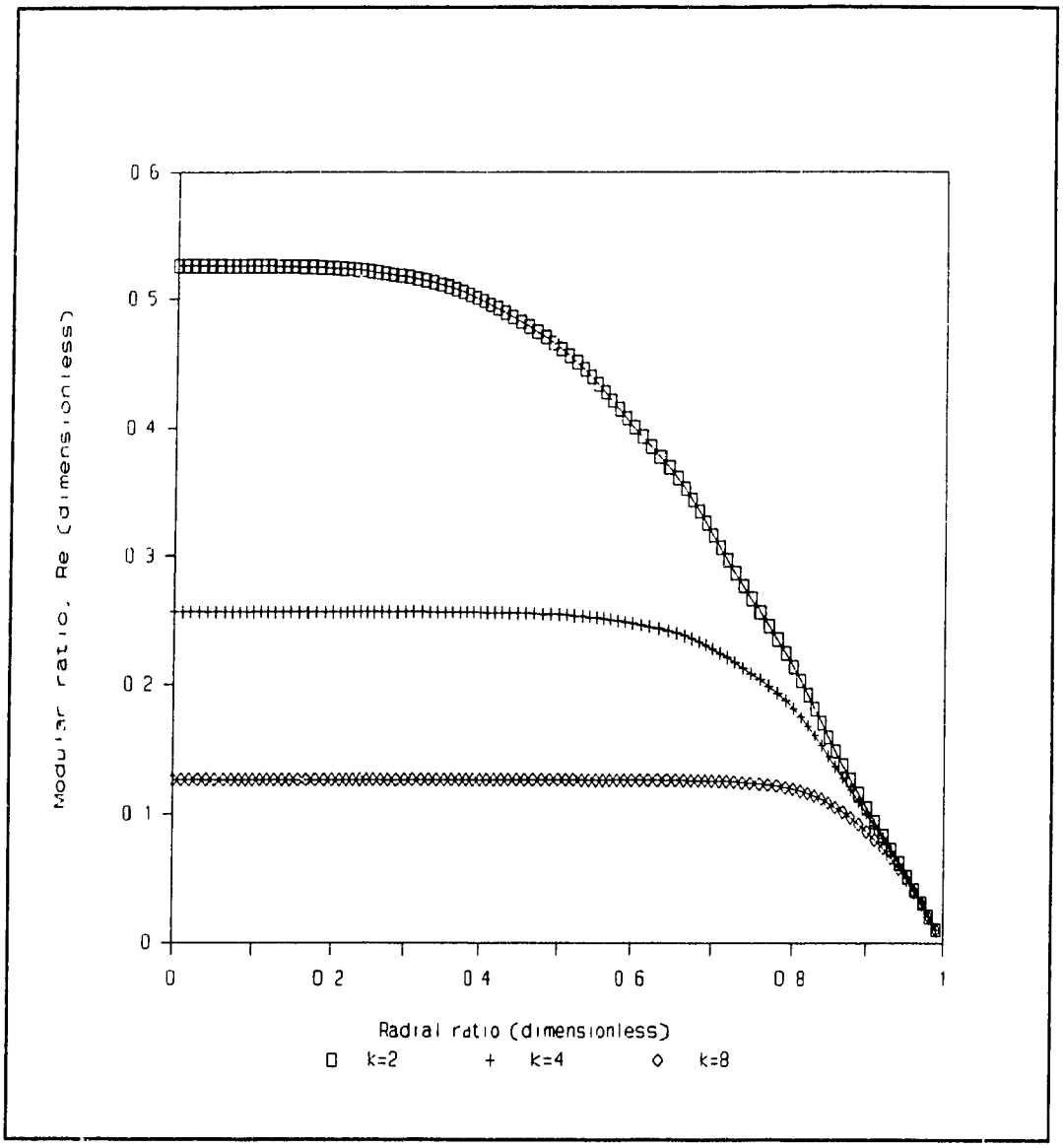

Fig. 2.16: Graph of ratio of effective core modulus to elastic tangential modulus, R_e, versus radial ratio, a/b, for anisotropic linear materials with k values of 2, 4 and 8, with Poisson's ratio = 0.1 for all three cases.

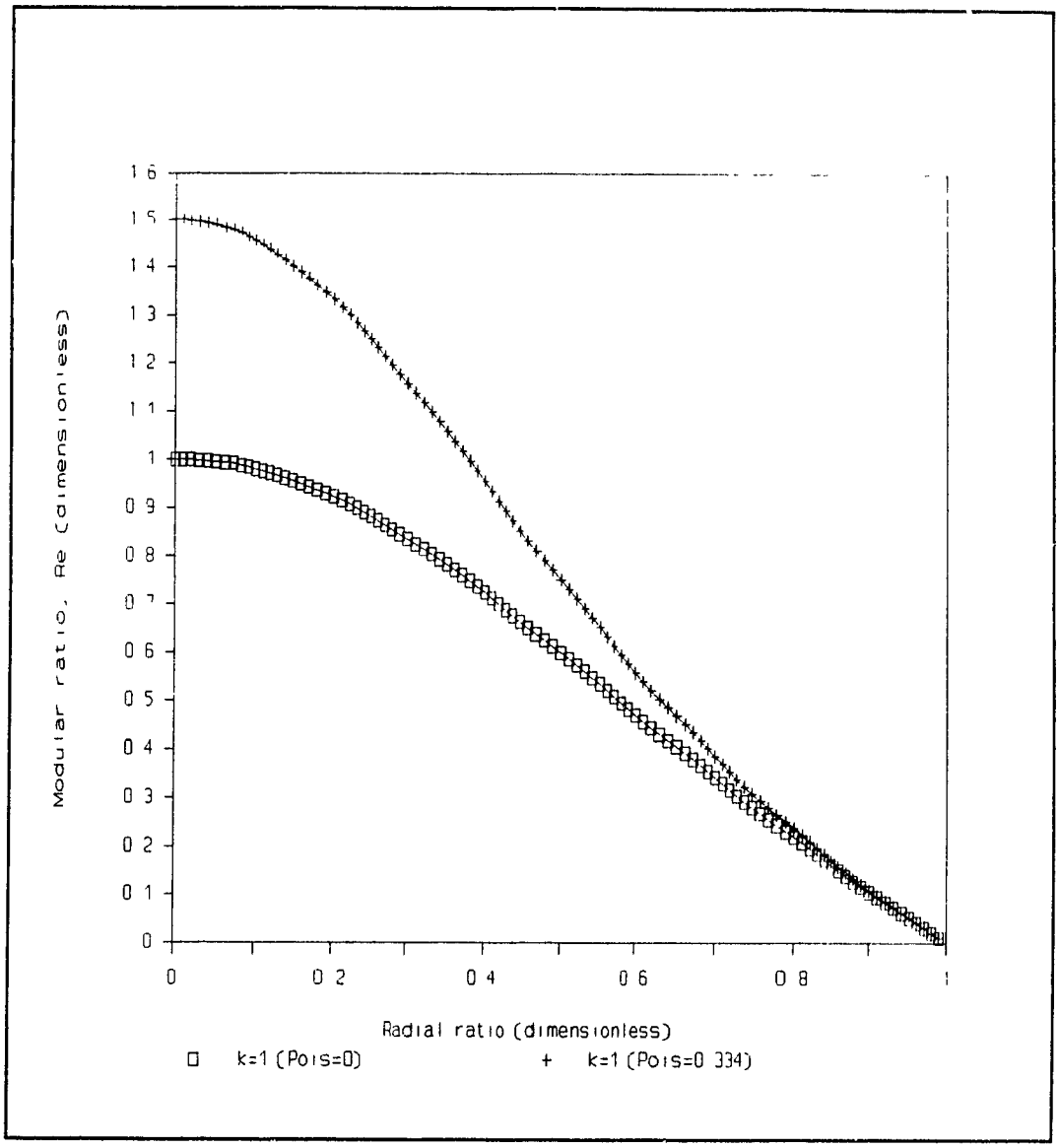

Fig. 2.17: Graph of ratio of effective core modulus to elastic tangential modulus, R_e, versus radial ratio, a/b, for isotropic, linear core materials with Poisson's ratio of 0.0 and 0.334.

2.5.4.2 The Core-Roll Winding System: Sensing The Presence of The Core Through Layers of Wound Material

Having determined the effective core elasticity modulus, we next wish to know how the hardness (or softness) of the core material will be obscured by the build-up of roll material over it. This is necessary in order to incorporate the radial variation of the hardness effect into a roll winding model. Intuitively, one would expect such a curve of hardness to start with the core stiffness modulus at core radius, then change quickly with radius, and finally end up at many multiples of the roll radius with a value approaching that of the roll material itself [9].

The general arrangement for a two-body core and roll material is diagrammed in Fig. 2.10. Referring to the latter figure, a and b denote the inner and outer core radii, respectively; and d denotes the roll outer radius. The radial deformations u_b (at radius b) and u_d (at radius d) are caused by the test pressure, p, applied at radius d. The radial deformations at radii b and d can be determined from equations (2.41) provided that the external and internal pressures, q and p, can be established for each ring. The boundary conditions for each ring can then be used to obtain the missing information in equation (2.41). For the inner ring, the internal pressure, p, is zero,

while the external pressure, q_b, is that developed at the interface when the deformation becomes u_b (at r=b). For the outer ring the external pressure, q, is the test pressure applied, and the internal pressure at the interface, p_b, exactly equals q_b for the inner ring. Also the outer ring's radial deformation at the interface radius b is equal to that of the inner ring. Noting that c in equation (2.41) applies when r is between a and b (see Fig. 2.15), thus for the inner ring c_1 is used to denote the radial ratio and similarly; c_2 is used for the outer ring. Further, the variable b in equation (2.41) refers to the outer radius, and hence d should be used in its place in the case of the outer ring. By setting the two deformations, u_b, of the inner and outer rings equal; the following solution is obtained for p_b, the pressure at the interface, in response to an external pressure, q:

$$p_b = q \frac{\dfrac{2k_2 c_2^{k_2-1}}{1-c_2^{2k_2}}}{\left[\dfrac{k_2(1+c_2^{2k_2})}{1-c_2^{2k_2}}+\mu_{\theta_2}\right]+\dfrac{E_{\theta_2}}{E_{\theta_1}}\left[\dfrac{k_1(1+c_1^{2k_1})}{1-c_1^{2k_1}}-\mu_{\theta_1}\right]}, \qquad (2.45)$$

where all quantities are as defined earlier. However, those quantities subscripted ($_2$) refer to the roll material parameters; whereas those subscripted ($_1$) refer to the core material parameters. As it is apparent from above, we are incorporating the anisotropy effects in both roll and core materials.

The analytic equations developed thus far for predicting the radial deflections at the outer roll radius and at the roll/core interface, the pressure at the interface and the effective elasticity modulus; based on applying the analysis of generalised plane stress for an annular plate possessing cylindrical anisotropy, can be used to compare the results obtained from the finite-element analysis of the solid core-roll system. The case to be studied via the analytic approach is that used for the finite-element model; namely, a solid core with radius b=1" (2.54 cm), $E_{\Theta 1}=30\times10^6$ psi (206.7 GPa), $\mu_{\Theta 1}=0.292$, $E_{\Theta 2}=100,000$ psi (689 MPa), $\mu_{\Theta 2}=0.05$, q=100 psi (689 kPa) and $k_1=k_2=1$ (both core and roll materials being isotropic). Table 2.5 shows the computed values for the radial deformation at the roll outer radius, u_d, the effective roll modulus, E, at the outer roll radius d, the radial deformation at the core/roll interface (at radius b), u_b, and the interface pressure, p_b; each being computed at roll outer radii 1.5", 2.5", 3", 3.5" and 4". The close agreement between the numerical results of Tables 2.4 (finite-element output) and 2.5 confirm the accuracy of the algebraic solution (equations (2.41)-(2.45)).

The modulus values shown in Table 2.5 are decreasing with greater distance from the core, as expected. For large radial ratios, it was expected that the asymptote would approach the roll material value. (It should

approach $100,000/(1-\mu_{\Theta 2}) = 105,263$ psi.) The pressure at the core however, keeps rising as the radial ratio grows, arriving at approximately 1.8 times the test pressure when $c_2=4$ (roll outer radius=4"). This is an artifact of the isotropic condition; when winding actual materials one seldom finds equal radial and tangential moduli [9].

The analytical approach can further be used to solve test cases for different anisotropic ratios, and the results are plotted in Fig. 2.18. In this figure an aluminium core is modelled, having radial ratio, $c_1=0.80$, elasticity modulus, $E_{\Theta 1}=10^7$ psi, Poisson's ratio, $\mu_{\Theta 1}=0.334$. The roll material's tangential modulus is held constant at a value of 600,000 psi, typical both of paper and polyester film; whilst the radial modulus is found by dividing this value by k^2. The latter figure may seem to be rather high, however, one ought to bear in mind that the radial Poisson's ratio, μ_{r2}, will be equal to $(\mu_{\Theta 2}/k^2)$, which will agree with the range of values typically measured during stack tests of compressible sheet material.

Fig. 2.18 demonstrates that the ability to detect the presence of a hard core by modulus measurements made at the exterior surface becomes all but impossible at radial ratios of 2.5 or greater, whenever the anisotropy ratio, k, is 8 or greater. This is within the normal range of k values for paper and many plastic film materials. The range of k from 2 to 8 would apply to plastic film

materials with very high radial elasticity modulus, E_r, and particularly those with low tangential modulus, E_Θ, on the order of 150,000 psi. Winding materials having $E_r=E_\Theta=600,000$ psi are harder to find [9].

The analysis developed thus far has only enabled us to predict in a linear anisotropic material of constant radial elasticity modulus, how strongly the core properties can be sensed at different distances from the core. Indeed, an appreciation of how rapidly the core effect can fade away when k is large is given upon examining Fig. 2.18; nonetheless, this is not all that happens when a roll is wound. The initial layers which are added over a hard core also present a hard interface to the layers added, because of the stiffening effect of the core underneath. It would be much too complicated to develop a predictor equation which takes into account the continuous change of the anisotropy ratio, k, with radius as more layers are added.

In Chapter Three, the final one of this Thesis, we shall endeavour to make the necessary adjustments for roll material stiffness parameters. We shall further incorporate such adjustments to modify the existing energy-balance roll structure formulae developed by J. D. Pfeiffer [5,6].

Table 2.5: Numerical results obtained from analytic equations (2.41)-(2.45)

Core-Roll Parameters

* Core outer radius, b=1" (2.54 cm)
* Effective core modulus=30×10^6 psi (206.7 GPa)
* Core's Poisson's ratio=0.292
* Roll's elasticity modulus=100,000 psi (689 MPa)
* Roll's Poisson's ratio=0.05
* Uniform external pressure applied at outer roll radius=100 psi (689 kPa)

Radius d (in)	u_d ($10^{-3}\times$in)	E (psi)	u_b ($10^{-6}\times$in)	p_b (psi)
1.5	-0.5675	264,306	-3.2032	135.73
2.5	-1.7453	143,239	-3.9203	166.12
3.0	-2.3043	130,193	-4.0772	172.76
3.5	-2.8457	122,994	-4.1786	177.04
4.0	-3.3737	118,563	-4.2460	179.92

N.B. i) radius, d = roll outer radius,

ii) u_d = radial deformation at radius d,

iii) E = effective roll modulus at radius d,

iv) u_b = radial deformation at core outer radius b,

v) p_b = radial pressure at core/roll interface, and

vi) minus signs represent inward deflections.

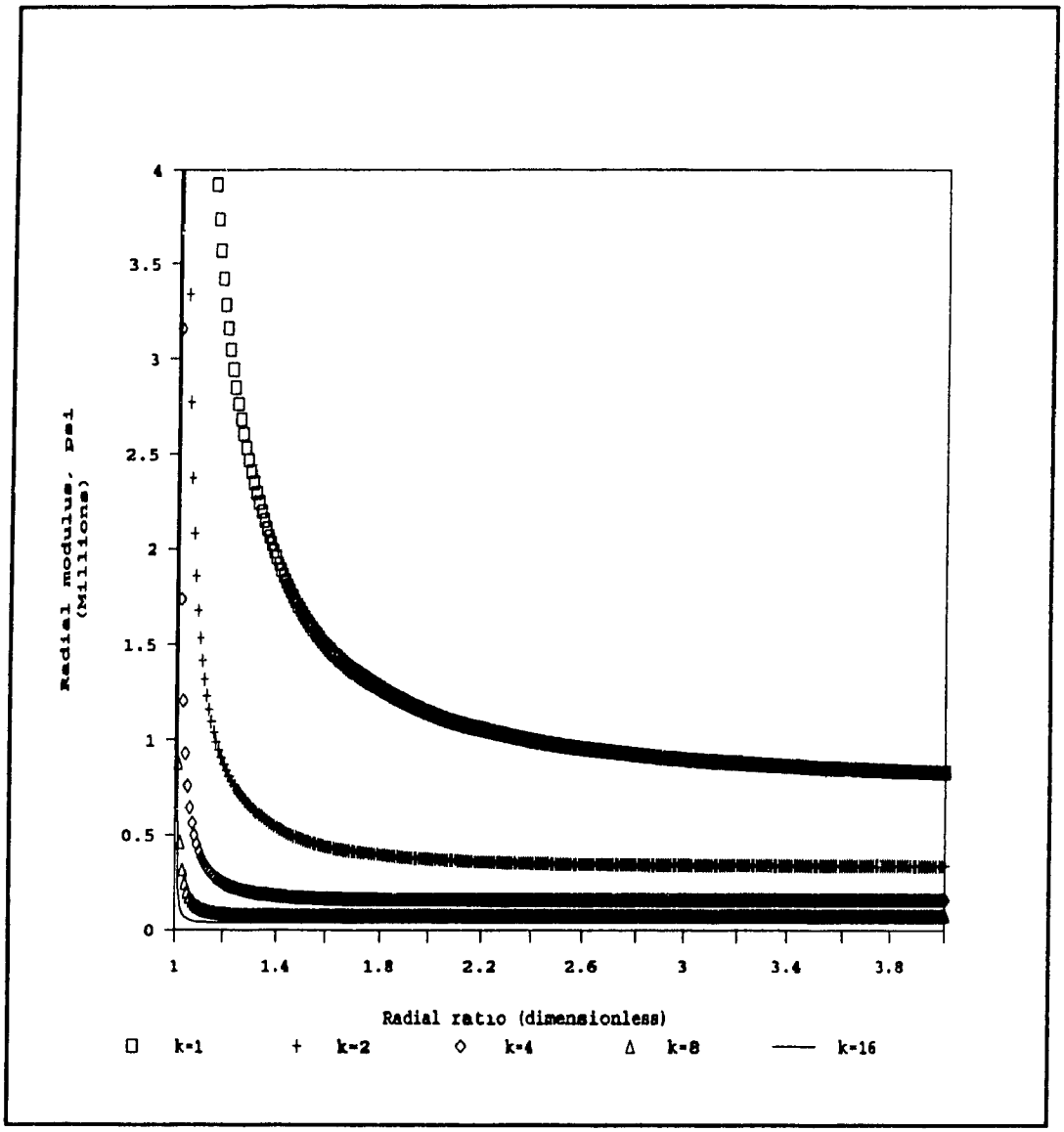

Fig. 2.18: Variation of radial modulus with distance from the core for various ratios of k. Core aluminium: a=0.8, b=1. Roll material: E_θ=600,000 psi, μ_θ=0.2, E_r values depend upon k.

CHAPTER THREE

MODIFICATION TO ENERGY-BALANCE ROLL STRUCTURE FORMULAE

3.1 INTRODUCTION

For a roll of paper or plastic film being wound, energy-balance principles were used to calculate roll structure under a given pattern of wound-in tension for materials that are non-linear in compression behaviour [5,6]. This is analogous to the actual winding process, in which the tensile strain energy put into elements of the web by the web-carrying tension, provides the energy necessary to compress the layers underneath into a firm cylindrical roll body.

Pfeiffer's two-parameter model [5,6], which has been studied extensively in Chapter One, results in the slope of the pressure versus strain curve having linear dependence on the pressure itself:

$$P = -K_1 + K_1 \exp(K_2 \varepsilon_r), \tag{3.1}$$

where, P = inter-layer pressure, in Pa or psi,

K_1 = pressure multiplier, in Pa or psi,

K_2 = basic springiness factor, dimensionless, and

ε_r = radial compressive strain, dimensionless.

$$\therefore \quad \text{slope} = dP/d\varepsilon_r = K_1 K_2 \exp(K_2 \varepsilon_r). \tag{3.2}$$

And recognising that

$$K_1 \exp(K_2 \varepsilon_r) = P + K_1; \tag{3.1'}$$

then,

$$dP/d\varepsilon_r = K_2(P+K_1) = K_2 P + K_1 K_2. \tag{3.3}$$

The latter equation shows that the slope of the curve is a linear function of P with a constant additive term of $K_1 K_2$.

Equation (3.3) gives the local modulus of elasticity around the P, ε_r operating point.

The energy-balance scheme does not require repeated iterations of the winding structure from the core outward every time an incremental thickness of wind is added to the outer radius. Instead, a single pass is made to calculate the roll residual inter-layer pressure and tangential stress, beginning at the outer roll radius and moving to the core. The energy in a unit volume of a web is calculated, based on the winding tension and tangential elasticity modulus of the web, E_t. This energy appears inside the roll body as a combination of the energy necessary to produce non-linear compression of the sheet material up to the inter-layer pressure, and the energy associated with the residual tangential stress within the roll. The combination is calculated using distortion energy theory [5,6]. The rate of change of pressure with radius, $d\sigma_r/dr$, is limited by the hoop stress equation; viz.,

$$\sigma_t - \sigma_r - r(d\sigma_r/dr) = 0,$$

to be that which is allowable under the current values of radial and tangential stresses, σ_r and σ_t, to keep the equation in balance.

Nothing mentioned so far in the description of the energy-balance solution method gives the winding program[1]

[1] written by J. D. Pfeiffer ©.

a warning that the stiffening effect of the core is soon to be felt, as the program makes evaluations of the winding tension level as the solution proceeds directly from the roll outer radius to the core radius. In the existing program, the solution reaches the core at a value intended to be correct for winding on an infinitesimally small core of a zero-approaching radius. However, this is wrong if we are to simulate the interface with a hard or a soft core.

In the next section, we shall attempt to rectify this situation by incorporating Chapter Two's findings in order to enable the existing winding program to account for core stiffening.

3.2 EMPLOYING RADIAL STIFFNESS MULTIPLIERS TO ACCOUNT FOR CORE STIFFENING

The approach that is recommended to work with the energy-balance solution is patterned on how the web actually responds during winding in the zone adjacent to the core [9]. The first several wraps laid against a hard metal core cannot easily be moved radially by the pressure developed by wraps laid on top. If they could deform radially inward towards the roll centre, the rapidly changing tangential strain would cause them to lose their initial tension, just as wraps in the outer roll body do. But the stiffness of the core prevents them from moving inwards, so they behave as if their radial modulus, E_r, has been artificially increased by the presence of the core.

In an attempt to incorporate the vast difference of material properties, which is a must if a valid approach to the solution of the roll winding problems is sought; Pfeiffer [8] modified his earlier two-parameter model to include a third term, a linear function of strain, characterised by one additional constant strain multiplier: K_3, in Pa or psi. Pfeiffer's modified equation for measuring the compressive stress-strain behaviour of sheet material is,

$$P = -K_1 + K_1 \exp(K_2 \varepsilon_r) + K_3 \varepsilon_r, \qquad (3.4)$$

where all variables are as defined earlier. The slope, which is nothing other than the roll body's radial

elasticity modulus, E_r; then becomes

$$E_r = dP/d\varepsilon_r = K_1K_2 \exp(K_2\varepsilon_r) + K_3. \quad (3.5)$$

And further substituting $K_1 \exp(K_2\varepsilon_r)=P+K_1-K_3\varepsilon_r$ into equation (3.5) we will obtain,

$$E_r = dP/d\varepsilon_r = K_2P + K_1K_2 + K_3(1-K_2\varepsilon_r). \quad (3.6)$$

Equation (3.5) is most readily evaluated if ε_r is known. Integrating equation (3.5) and making use of the pressure versus strain equation (3.4) and finally, taking the natural logarithm of the resulting equation; we will get a relation which will enable us to solve for strain when pressure is known, viz.,

$$\varepsilon_r = \{\ln[(P+K_1-K_3\varepsilon_r)/K_1]\}/K_2. \quad (3.7a)$$

Since ε_r appears on both sides of equation (3.7a), one must use successive re-iterations in order to evaluate the above relation. This is done by writing equation (3.7a) as

$$\varepsilon_r^{(1)} = \{\ln[(P+K_1-K_3\varepsilon_r^{(0)})/K_1]\}/K_2, \quad (3.7b)$$

evaluating the latter expression and setting $\varepsilon_r^{(0)}=\varepsilon_r^{(1)}$; then repeating this process several times until $\varepsilon_r^{(0)}$ and $\varepsilon_r^{(1)}$ are essentially equal. (If we start $\varepsilon_r^{(0)}$ at zero, then, the convergence is proved to be rapid.)

To model the effects shown in Fig. 2.18 (of Chapter Two) where the tangential elasticity modulus, E_t, is much greater than the radial modulus, E_r; a function is required which will cause a high slope of the stiffness parameter near the core. Thus a multiplier, γ, is introduced which is used to raise or lower E_r [9]. This multiplier is used

on both K_2 and K_3, but not K_1. The form for calculating γ is given by

$$\gamma = 1 + [F_1/(R-\beta)^{\Theta}], \tag{3.8}$$

where F_1, β and Θ are dimensionless quantities which will be determined below; and R is the dimensionless ratio of roll radius to core radius. Hence the compressive stress-strain equation will read,

$$P = -K_1 + K_1 \exp(\gamma K_2 \varepsilon_r) + \gamma K_3 \varepsilon_r. \tag{3.9}$$

And the slope, E_r, becomes

$$E_r = K_1 \gamma K_2 \exp(\gamma K_2 \varepsilon_r) + \gamma K_3. \tag{3.10}$$

In expression (3.8), Θ is usually taken as 1, however, in the event other values such as 1.5 or 2 are chosen; Θ will be included in the procedure for evaluating the other coefficients. Equation (3.8) is capable of modelling the effects illustrated in Fig. 2.18 if β is made slightly less than 1, and F_1 is positive [9]. By contrast, when winding on a soft core with effective elasticity modulus, E_c, slightly lower than E_r, F_1 will be negative to soften the roll body; and β will be considerably less than 1, near zero or negative. F_1 and β depend on γ_0, which is the value of γ at the core surface, and a slope SL, which is $d\gamma/dR$ at the core, and an intercept. The equations for these relationships are given below, where P_o is the "no-core[1]"

[1] The "no-core" pressure, P_o, is the residual pressure value when calculations, provided that winding tension values are to avail, are continued down to a radius of zero without ever acknowledging the presence of the core.

pressure that would exist at the core radius if $\gamma=1$ for all radii.

$$F_2 = E_c/E_r = E_c/(K_2P_o), \tag{3.11}$$

$$k^2 = E_t/E_r = E_t/(K_2P_o), \tag{3.12}$$

$$\gamma_o = N_1[1 - \exp(-F_2/N_2)], \tag{3.13}$$

$$SL = 2k^2[N_3 + (N_4/(F_2+N_5))], \tag{3.14}$$

$$\beta = [\theta(\gamma_o-1)/SL + 1],$$

$$= [(\gamma_o-1)/SL + 1]_{\theta=1}, \tag{3.15}$$

$$F_1 = -SL(1-\beta)^{\theta+1}/\theta,$$

$$= -[SL(1-\beta)^2]_{\theta=1}, \tag{3.16}$$

where the dimensionless empirical constants used above are:

$N_1=25$ $N_2=27.972$ $N_3=-16.31755$

$N_4=80.12425$ $N_5=4.43017$.[2]

It is worthy of note that approximating E_r by (K_2P_o) in equations (3.11) and (3.12) is a short cut to using equation (3.5). The results of the approximation, being only a few percent low, are sufficient for estimation of stiffness parameter effects; especially when the constants N_1-N_5 can be adjusted to compensate. The determination of P_o is the most difficult step, requiring several iterations to find a balance between the equal quantities; the radial and tangential stresses σ_r and σ_t, just outside the core radius, where we assume the rate of change of pressure with

---

[2] The empirical constants, N_1-N_5, were developed [9] by fitting results to some known solutions of the roll winding problems which use the method developed by Dr. Z. Hakiel of Eastman Kodak Co., New York, U.S.A. [15].

radius, $d\sigma_r/dr$, is zero. The procedure for determining P_0 necessitates that we indulge in explaining some other variables and relevant concepts, as follows.

When a stack of sheet material is compressed from zero pressure to a finite compressive strain, the work done per unit volume is equal to the area under the stress-strain curve from zero up to that point. Hence, denoting the energy involved in compressing the roll material up to radial strain ε_r, by the symbol ξ_r in units J/m^3; we will get by integrating equation (3.4):

$$\xi_r = -K_1\varepsilon_r + K_1[\exp(K_2\varepsilon_r)-1]/K_2 + K_3\varepsilon_r^2/2. \qquad (3.17)$$

But to calculate the total stored energy on a distortion-energy basis [5,6]; a winding stress, denoted by σ_e, that has an energy level equivalent to the local pressure σ_t and is a linear equivalent of the non-linear compression response, must be calculated using

$$\sigma_e = -(2\xi_r E_t)^{1/2}, \qquad (3.18)$$

where all symbols are as defined before.

The magnitude of the energy input per cubic volume unit, denoted by ξ_w in units J/m^3, coming to the roll in the form of elastic strain in the web because of its wound-in tensile stress, σ_w, is given by:

$$\xi_w = \sigma_w^2/2E_t. \qquad (3.19)$$

On the outside of the roll, where the residual tension is positive and the pressure is low, most of this energy will be tensile in nature. Interior sections of the roll, which

used to be on the outside, have been compressed radially, and residual tension has been reduced. In these sections, most of the energy from σ_w has been converted into compressive energy. The premise that tension disturbances or variations stay close to the location at which they occurred [5], holds true in our analysis.

Thence, an initial approximation for the "no-core" residual pressure, P_0, can be obtained from

$$P_0^{(0)} = (\sigma^2_w K_2)/(2E_t). \tag{3.20}$$

Furthermore, Pfeiffer [5,6] uses the distortion-energy theory to obtain the von Mise's equivalent stress, σ', from the compression equivalent stress, σ_e, and the residual tensile stress, σ_t, as

$$\sigma' = (\sigma_t^2 - \sigma_e\sigma_t + \sigma_e^2)^{1/2}. \tag{3.21}$$

Then the energy stored by the roll stresses, ξ_s (in units J/m^3), is calculated to be

$$\xi_s = (\sigma_t^2 - \sigma_e\sigma_t + \sigma_e^2)/(2E_t). \tag{3.22}$$

Equations (3.4), (3.17), (3.18) and (3.22) are evaluated several times until the unit stored energy ξ_s in the zone near the core is sufficiently close to ξ_w to stop the iterations. When a new estimate of pressure P_0 is made as defined by equation (3.4), it is also assigned (negatively) to σ_t, since the rate of change of pressure with radius, $d\sigma_r/dr$, is assumed here to be negligibly small (i.e. $\sigma_t = \sigma_r = -P_0$). The hitherto-described sequential iterations to determine P_0, can easily be programmed so as to obtain the

desired output as we shall see in the following section.

3.3 ROLL-WINDING EXAMPLES

Four examples are considered here [9]. In all of them, the tension is assumed to have no variation with roll radius, i.e., constant winding tension. Tables 3.1 and 3.2 illustrate the winding parameters used for the example cases, and the parameter determination for stiffness multiplier γ (i.e. equations (3.13)-(3.16)); respectively. As regards Table 3.1, values for the effective core elasticity modulus, E_c, were rounded off after having been computed according to equation (2.43b) (note that E_c here is the same as E_{eff} used in equation (2.43b)). The radial stiffness has, for all three cases, been expressed as a function of pressure in the form of a polynomial series; viz.,

$$E_r = A_0 + A_1P + A_2P^2 + \ldots, \qquad (3.23)$$

which is the form used by Dr. Z. Hakiel for handling non-linear compression [15]. Hakiel's winding model re-balances all of the residual stresses throughout the roll on each iteration of adding tensile wraps at the outside, and in this manner it is able to take into account the stiffening action of the core. The values of K_1, K_2 and K_3, for the four cases, to reproduce the same pressure versus strain behaviour as Hakiel's were obtained by curve-fitting the polynomial series (equation (3.23)).

For each of the four cases, two diagrams are presented: one illustrating how the radial pressure, P_r,

varies with respect to the radial ratio, and the other demonstrates the variation of residual tensile stress, σ_t, with radial ratio. Three curves are shown in each diagram; one representing the modified energy-balance method solution, the other for Hakiel's winding model solution, and the last depicts the solution predicted by Pfeiffer's old energy-balance winding model without correction for core effects (i.e. when $\gamma=1$).

Fig. 3.1 corresponds to a condition where a polyester-type plastic film (high K_2 -or high A_1) is wound on a hollow metal core. The material parameters used are in agreement with those used in an example by Z. Hakiel published in 1987 [15]. However, the condition represented by Fig. 3.2 is more typical of paper wound on a metal core. The material properties demonstrated in Fig. 3.3 are similar to those of Fig. 3.1, except for the inclusion of a high A_0 term in the polynomial expression, and the fact that winding takes place at a lower constant tension. This example is from a recent publication by A. Penner [17]. In Fig. 3.4 a moderately stiff polyester film is wound tightly on a fibre core, causing large amounts of core deformation and the formation of high negative tangential stress just above the core. The energy-balance solution method prints out a warning message near the inflexion point of Fig. 3.4b at radial ratio 1.3 that buckling is likely to occur.

Table 3.1: Winding parameters for the three roll-winding example cases of section 3.3

(**N.B.** in all three cases the value of E_t=600,000 psi)

Case	1	2	3	4
E_c (psi)	890,000	890,000	890,000	46,000
σ_w (psi)	333.33	555.55	300.0	1000.0
A_0 (psi)	0.	0.	1060.	0.
A_1	1060.	124.	1060.	450.
A_2 (psi^{-1})	-0.153	0.0	0.0	0.0
K_1 (psi)	0.059600	0.056124	0.968729	0.056109
K_2	1049.88	124.006	1056.299	450.036
K_3 (psi)	-19.625	0.1875	-88.75	0.75

(**Note:** A_1 and K_2 values are almost equal.)

Table 3.2: Parameter determination for stiffness multiplier γ

Case	1	2	3	4
P_o (psi)	125.83	34.13	106.03	497.44
γ_0	5.35115	24.9864	6.18263	0.18297
SL	-83.052	-4520.85	-105.474	5.183
ß	0.9476093	0.9946943	0.9508633	0.8423482
F_1	0.279598	0.127264	0.254658	-0.128806

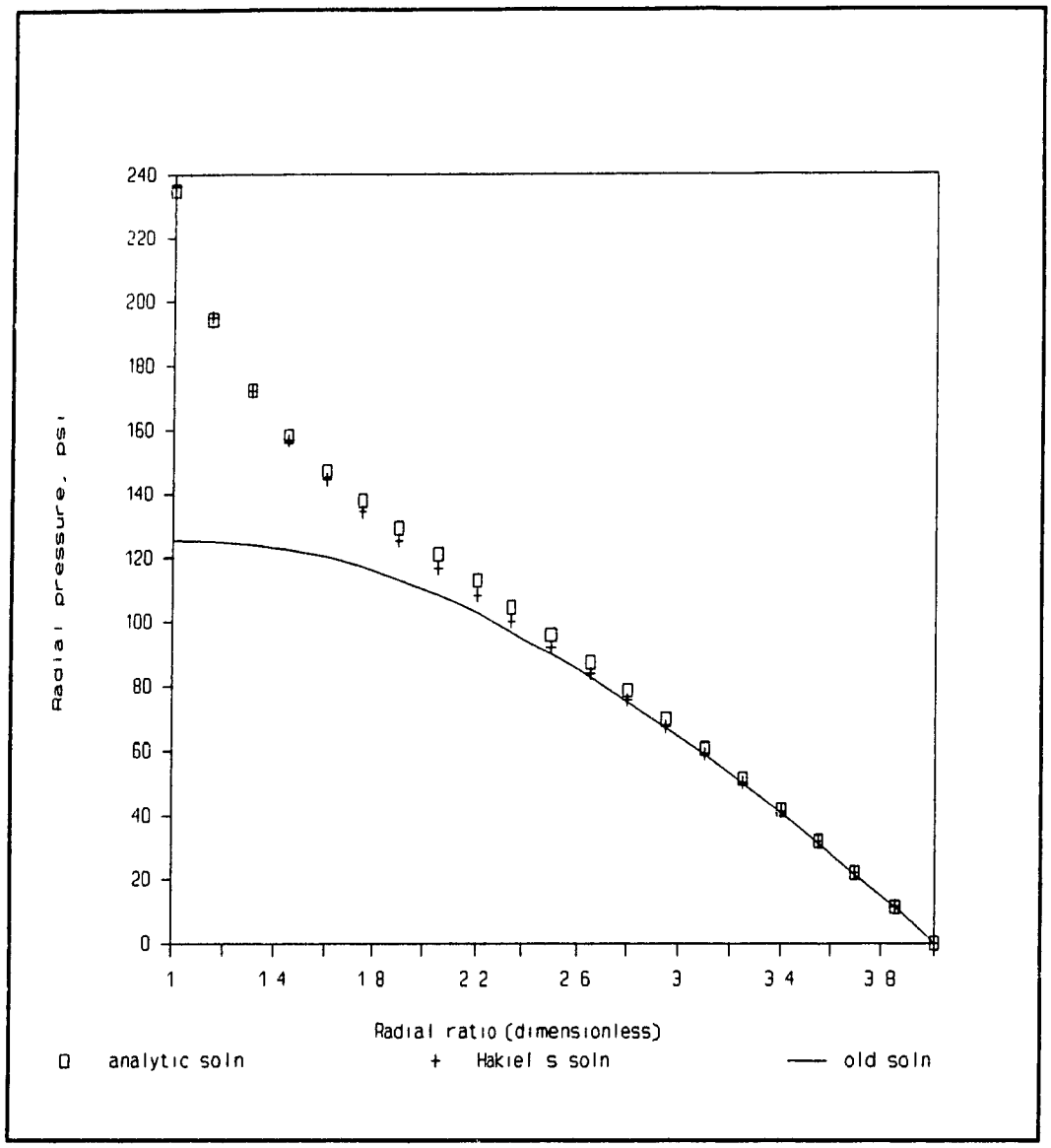

Fig. 3.1a: Graph of radial pressure versus radial ratio for case 1. (γ=1 curve assumes no core effects are present, i.e. Pfeiffer's old model.)

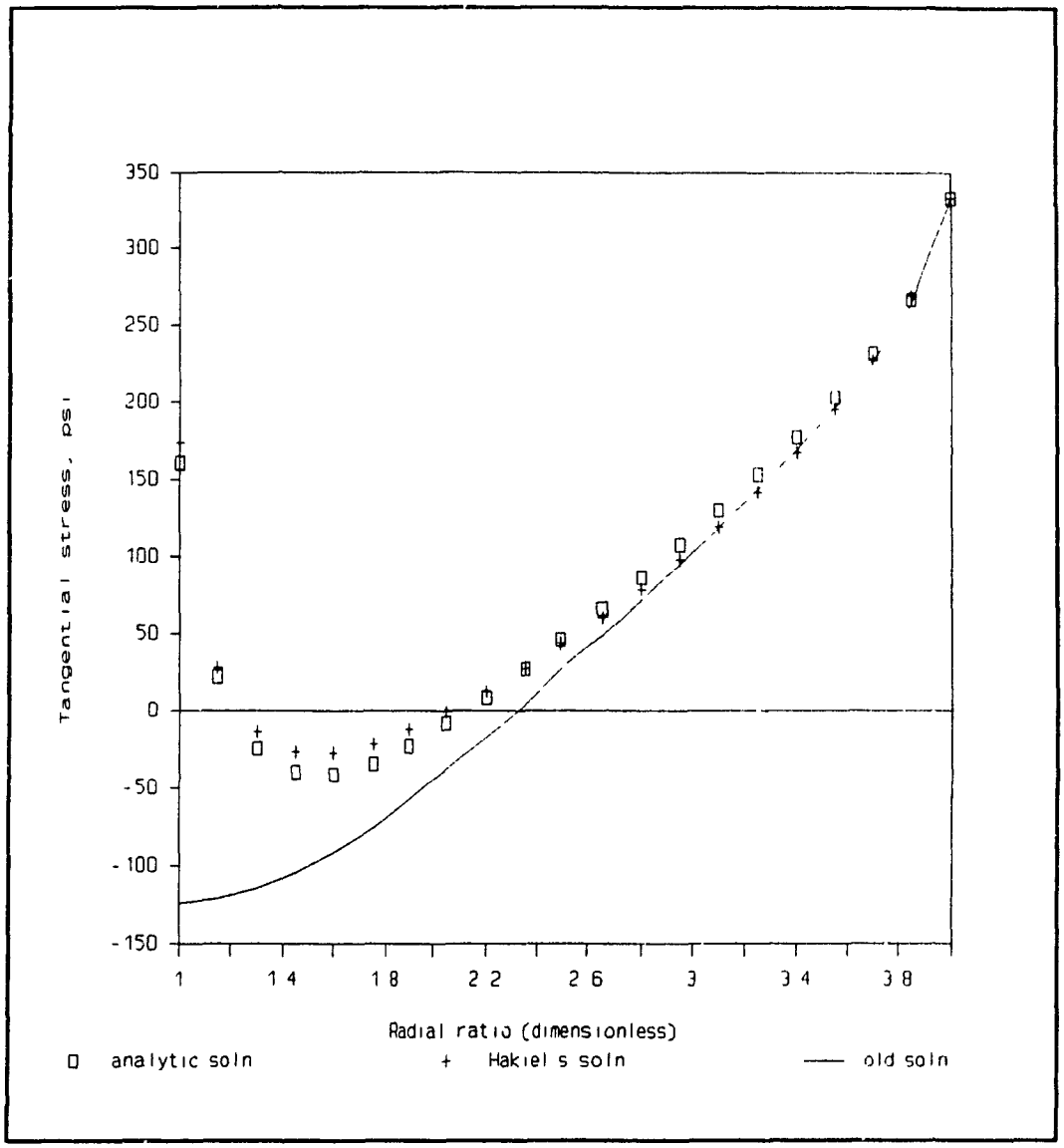

Fig. 3.1b: Graph of residual tangential stress versus radial ratio for case 1.

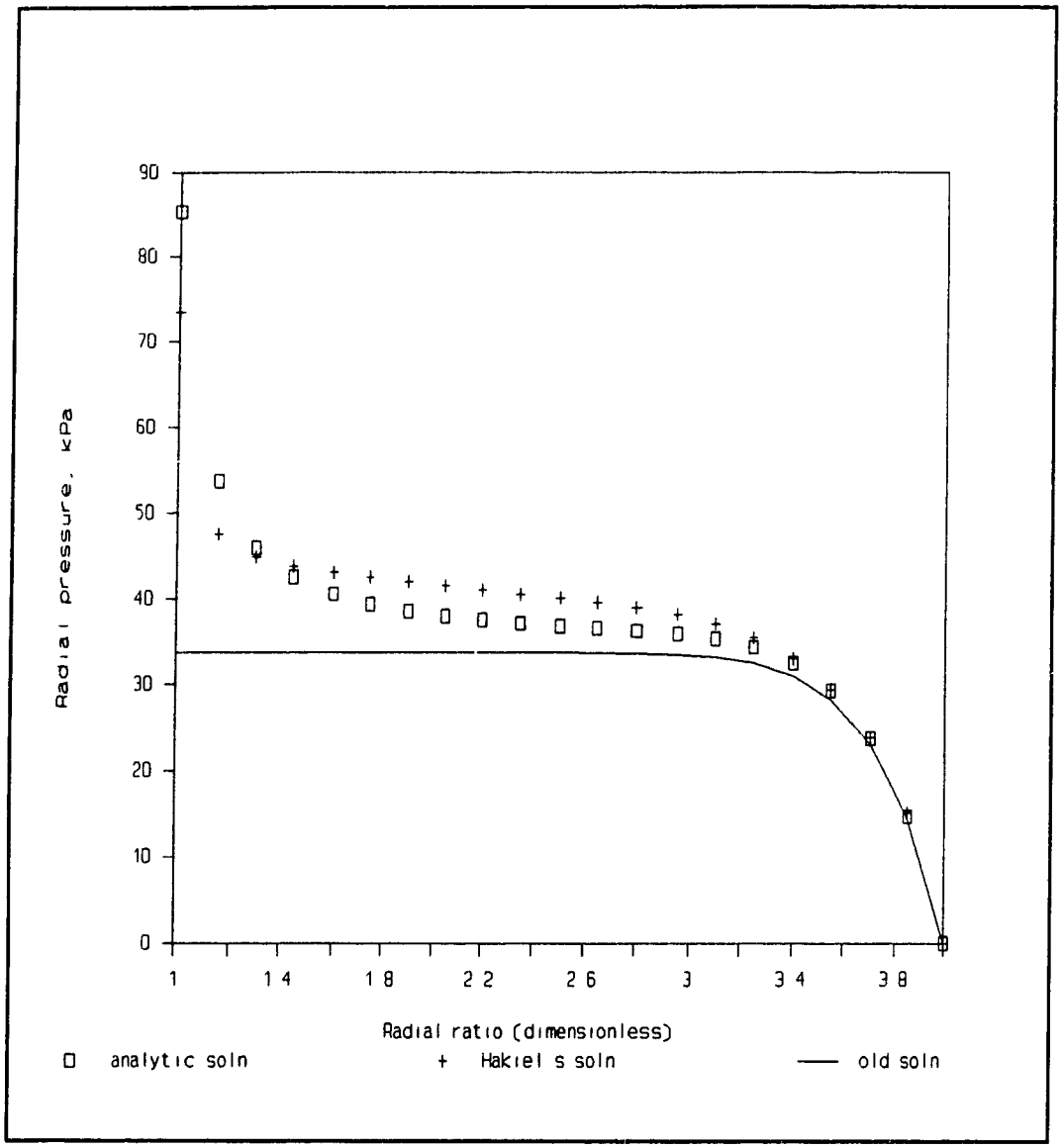

Fig. 3.2a: Graph of radial pressure versus radial ratio for case 2.

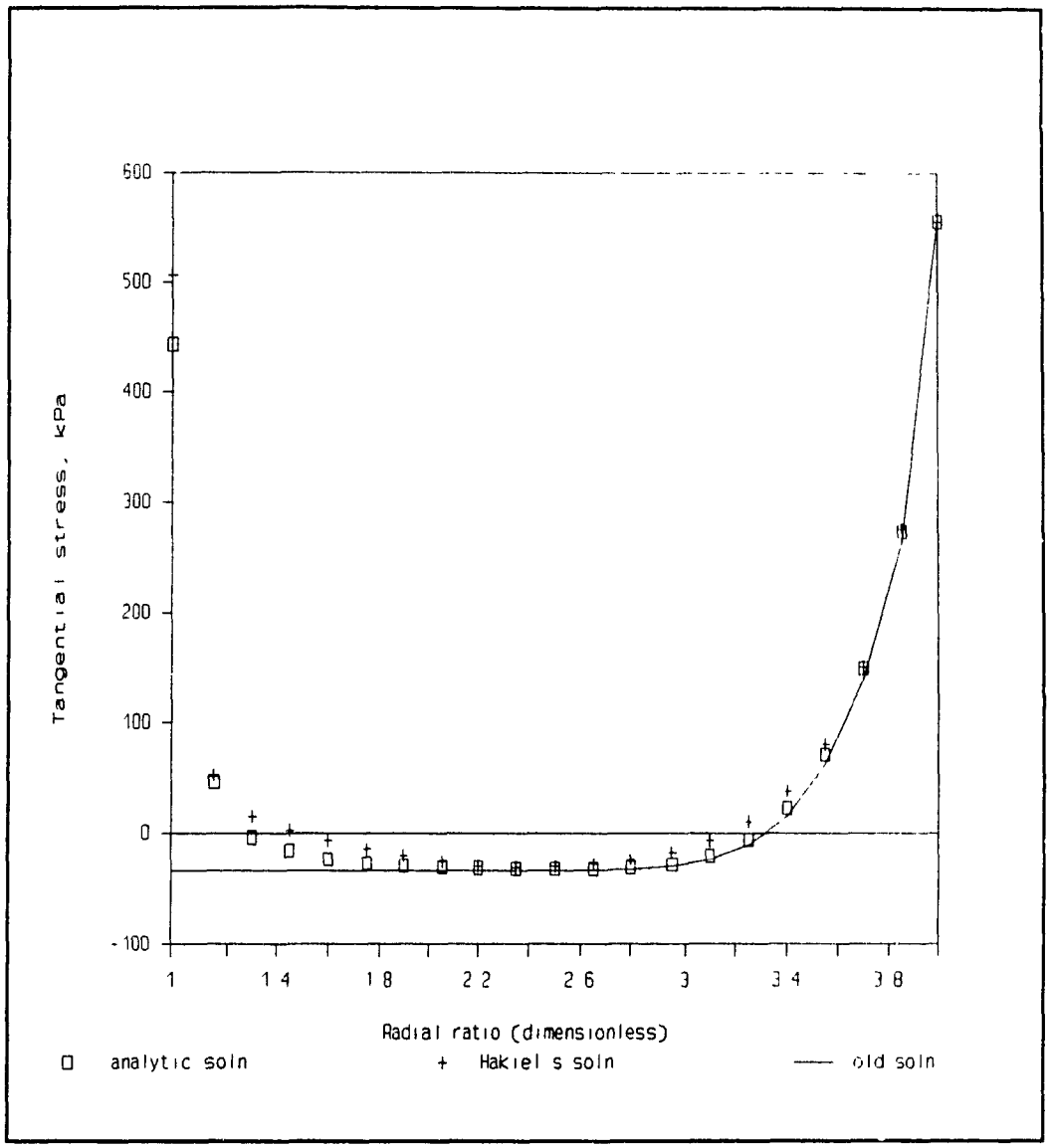

Fig. 3.2b: Graph of residual tangential stress versus radial ratio for case 2.

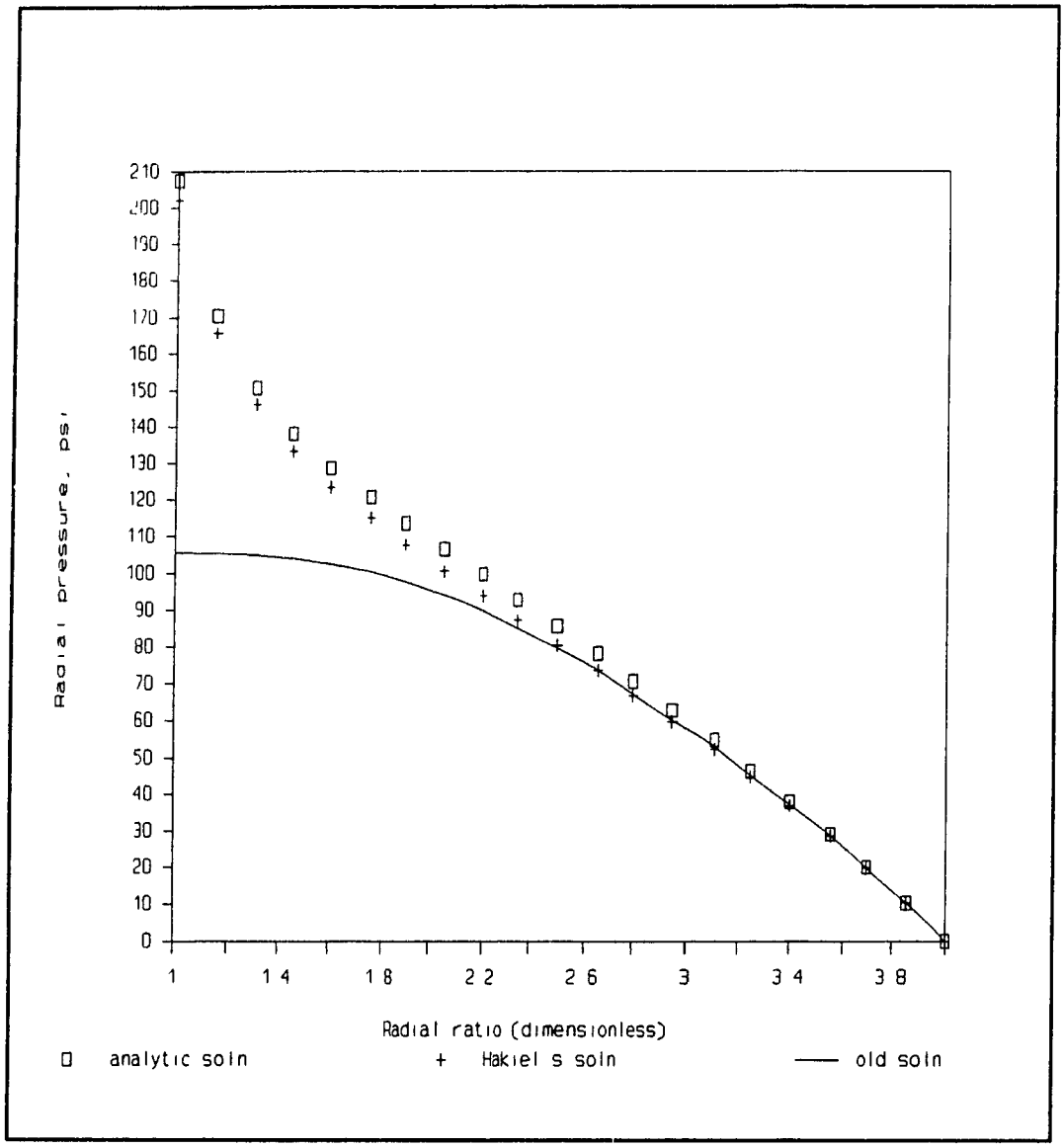

Fig. 3.3a: Graph of radial pressure versus radial ratio for case 3.

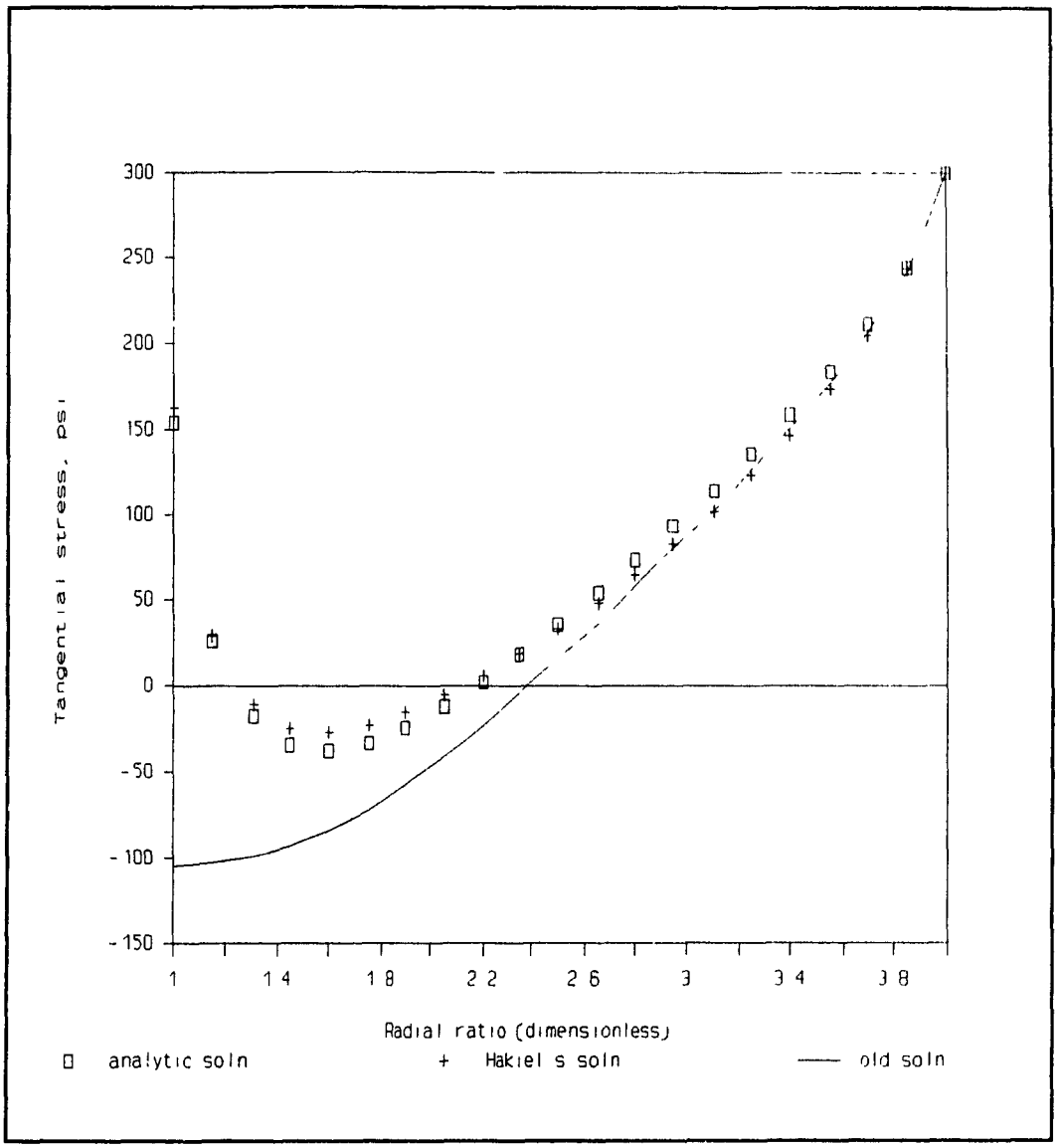

Fig. 3.3b: Graph of residual tangential stress versus radial ratio for case 3.

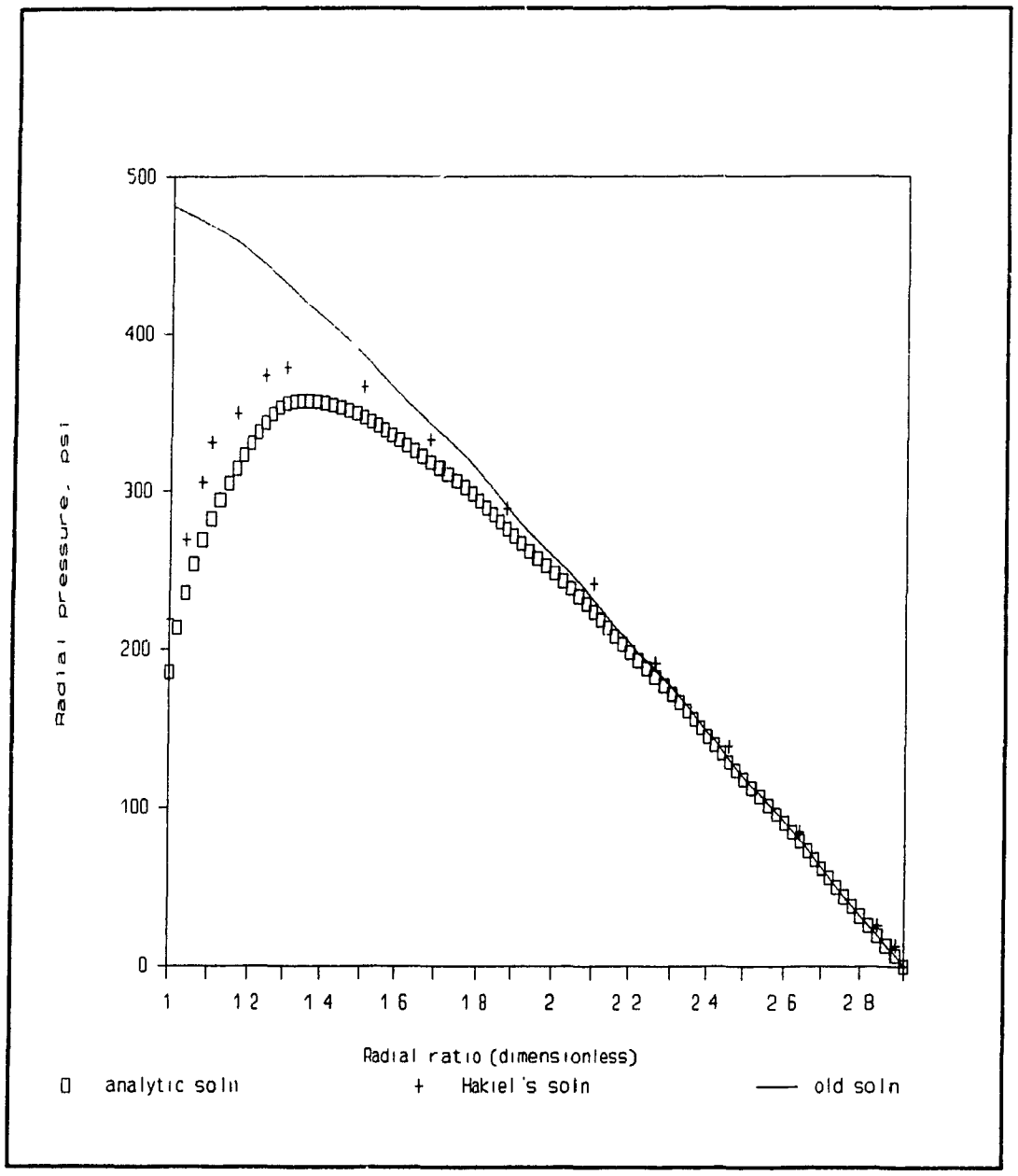

Fig. 3.4a: Graph of radial pressure versus radial ratio for case 4.

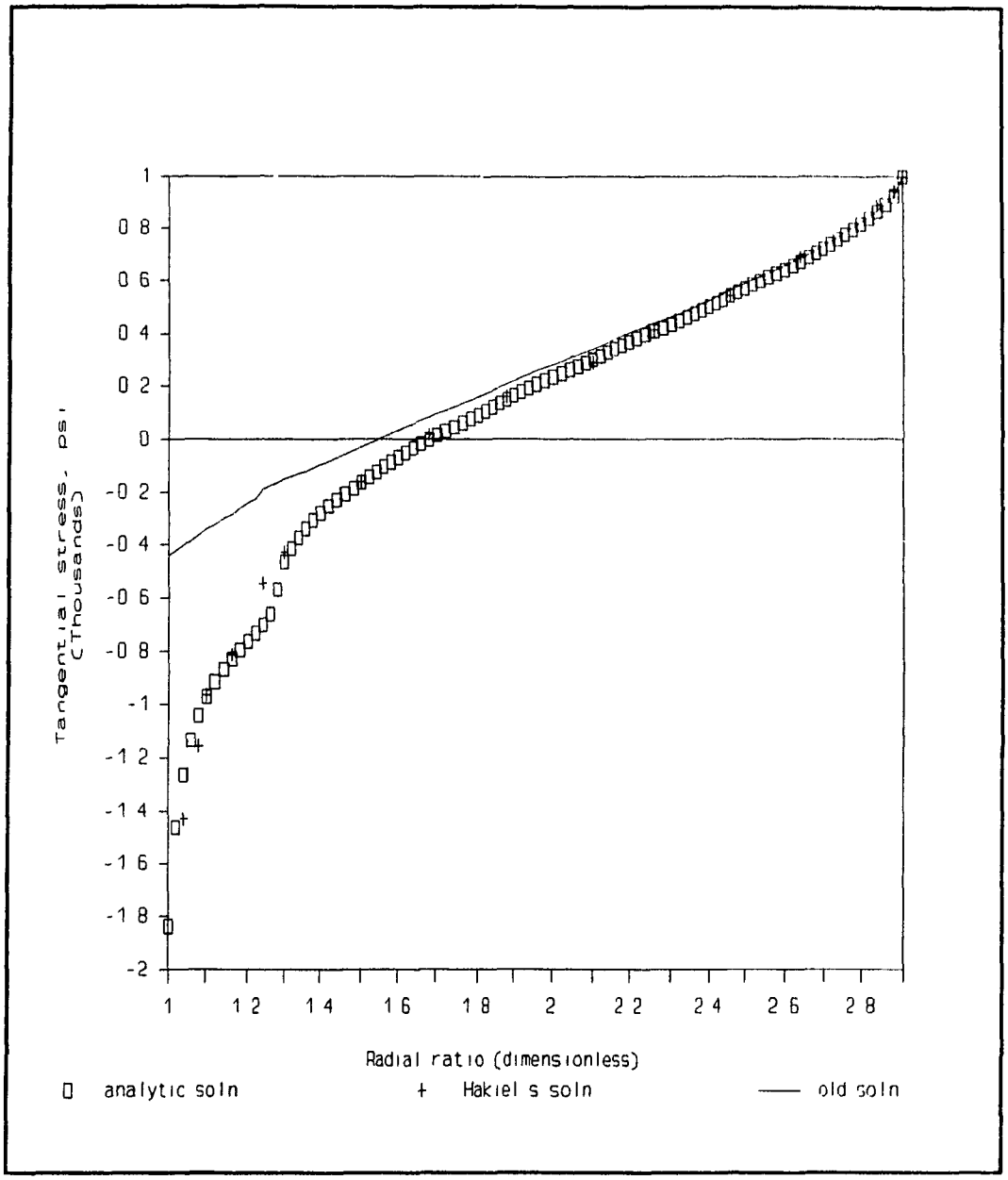

Fig. 3.4b: Graph of residual tangential stress versus radial ratio for case 4.

3.4 CONCLUSIONS

The progressive development in the line of analysis of how the core stiffness might influence the wraps of web material being wound around the core, as has been witnessed in some great detail in Chapter Two, led to realising the significance in the inclusion of the anisotropic behaviour of the web material as well as the core for the radial deformation of core structures and linear axisymmetric models. This made possible the prediction of effects, in core-roll winding systems, due to the application of pressure from the outside and the reaction from the underlayers which present a resistance to deformation.

The premise undertaken by Pfeiffer [5,6,8] in developing the energy-balance roll structure model; namely, that energy admitted to the roll does not migrate substantially in radial distance from the location at which it was applied, was undoubtedly confirmed by the analytic results of Chapter Two. In particular, the tremendous difficulty encountered when attempting to detect the presence of a hard core, by modulus measurements made at the outside surface at radius ratios of 2.5 or greater whenever the anisotropy ratio is relatively high (refer to Fig. 2.18). And, also, the precipitous attenuation of pressure predicted by the analytic equations for anisotropy ratios higher than 2.

The modifications performed on Pfeiffer's old energy-

balance model, based on Chapter Two's findings, agree reasonably well when compared to some known analytical solutions to core-roll winding systems. This agreement can further be improved upon, if and when data becomes available which can then be used to refine the five dimensionless constants (N_1-N_5) used to adjust the local effective radial elasticity modulus for the presence of the core.

CLAIMS TO ORIGINAL RESEARCH

The scope of originality in the course of this research principally encompasses the following:

1. the modelling and analysis of the core-roll system as an isotropic, flat platen model, to predict the influence of the core material's stiffness on layers of wound rolls,
2. performing compression testing and, subsequently, curve fitting the results to find equation types suitable for describing the material behaviour,
3. undertaking a linear, isotropic finite-element analysis of various axisymmetric core-roll models,
4. performing numerical analyses to search for equation types to fit Hakiel's solutions,
5. roll structure modelling for numerous forms of equations leading up to the final form of the stiffness multiplier, γ (many computer runs were made to investigate alternate exponential and power series forms that might be suitable), and
6. the in-depth study of curvilinear anisotropy and the rigorous analysis of the (generalised) plane stress of a body possessing cylindrical anisotropy, and the subsequent formatting of equations suitable for that type of solution.

SUGGESTIONS FOR FURTHER WORK

It should prove interesting to see what effects varying the radial elasticity modulus of the anisotropic material, has on the results obtained here. Moreover, attempting to consider the continuous change of the anisotropy ratio with radius as more layers are added in order to develop a predictor equation for the material's elasticity modulus, is a very complex and challenging task and may not prove feasible. However, it deserves some attention.

It is further suggested to perform experimental investigation of the type and distribution of stresses when winding high viscosity emulsions, coated on high modulus plastic sheet material; each of which having different temperature properties and subject to relaxation effects after winding. Finally, more data gathering is to be undertaken to see if the stiffness multiplier, γ, is suitable for all conditions encountered when many industrial materials are wound on a wide range of core types.

REFERENCES

1. Pfeiffer, J. D., "Internal Pressures in a Wound Roll of Paper," TAPPI Journal, Vol.49, №8, pp. 342-347 (1966).

2. Pfeiffer, J. D., "Mechanics of a Rolling Nip on Paper Webs," TAPPI Journal, Vol.51, №8, pp. 77A-85A (1968).

3. Pfeiffer, J. D., "Nip Forces and Their Effect on Wound-in Tension," TAPPI Journal, Vol.60, №2, pp. 115-117 (1977).

4. Pfeiffer, J. D., "Wound-off Tension Measurement in Paper Rolls," TAPPI Journal, Vol.60, №3, pp. 106-108 (1977).

5. Pfeiffer, J. D., "Prediction of Roll Defects from Roll Structure Formulas," TAPPI Journal, Vol.62, №10, pp. 83-85 (1979).

6. Pfeiffer, J. D., "An Update of Pfeiffer's Roll-Winding Model," TAPPI Journal, Vol.70, №10, pp. 130-131 (1987).

7. Pfeiffer, J. D., "Measurement of K_2 Factor for Paper," TAPPI Journal, Vol.64, №4, pp. 105-106 (1981).

8. Pfeiffer, J. D., "Surface Winding to Overcome The Strain Deficiency," TAPPI Journal, Vol.73, №10, pp.

247-250 (1990).

9. Pfeiffer, J. D., and Hamad, W. Y., "How Core Stiffness and Poisson's Ratio Affect Energy Balance Roll Structure Formulas," Proceedings of The First International Conference on Web Handling, Oklahoma State University, U.S.A., May 19-22, 1991.

10. Pfeiffer, J. D., "Effect of Rewinder Variables on Paper Smoothness," Presented at The 67th Annual Meeting of The Canadian Pulp and Paper Association, Montreal, Quebec, Jan. 26-30, 1981.

11. Pfeiffer, J. D., "Mechanics and Dynamics of Web Motion Between Spans," Proceedings of The 1987 American Control Conference, Minneapolis, U.S.A., pp. 2094-2099, June 10-12, 1987.

12. Pfeiffer, J. D., "Analysis of The Ring Patterns Formed When Periodic Disturbances Affect Roll Edges," TAPPI Journal, Vol.72, №10, pp. 59-65 (1989).

13. Pfeiffer, J. D., "Shear and Finishing in the supercalender Nip," University of Manchester Institute of Science and Technology Symposium on Supercalendering, Manchester, September, 1975.

14. Altmann, H. C., "Formulas for Computing the Stresses in Center-Wound Rolls," TAPPI Journal, Vol.51, №4, pp. 176-179 (1968).

15. Hakiel, Z., "Nonlinear Model for Wound Roll Stresses," TAPPI Journal, Vol.70, №5, pp. 113-117 (1987).

16. Penner, A., "Roll Structure Theory," TAPPI Journal, pp. 207-210, October, 1989.

17. Penner, A., "Roll Structure Calculations at Constant Wound-In Tension," TAPPI Proceedings, 1990 Finishing and Converting Conference, October 1990, pp. 105-110.

18. Tramposch, H., "Relaxation of Internal Forces in a Wound Reel of Magnetic Tape," Journal of Applied Mechanics, Vol.32, №4, pp. 865-873 (1965).

19. Tramposch, H., "Anisotropic Relaxation of Internal Forces in a Wound Reel of Magnetic Tape," Journal of Applied Mechanics, Vol.34, №4, pp. 888-894 (1967).

20. Yagoda, H. P., "Centrifugally-Induced Stresses Within Center-Wound Rolls - Part I," Mechanics Research Communications, Vol.7, №3, pp. 181-193 (1980).

21. Yagoda, H. P., "Centrifugally-Induced Stresses Within Center-Wound Rolls - Part II," Mechanics Research Communications, Vol.7, №4, pp. 233-240 (1980).

22. Yagoda, H. P., "Integral Formulas for Wound Rolls," Mechanics Research Communications, Vol.7, №2, pp. 103-113 (1980).

23. Yagoda, H. P., "Resolution of a Core Problem In Wound Rolls," Journal of Applied Mechanics, Vol.47, №4, pp. 847-854 (1980).

24. Yagoda, H. P., "Generalized Formulas for Stresses in Wound Rolls," TAPPI Journal, Vol.64, №2, pp. 91-93 (1981).

25. Willett, M. S., and Poesch, W. L., "Determining the Stress Distributions in Wound Reels of Magnetic Tape Using a Nonlinear Finite-Difference Approach," Journal of Applied Mechanics, Vol.55, №2, pp. 365-371 (1988).

26. Gerhardt, T. D., "External Pressure Loading of Spiral Paper Tubes: Theory and Experiment," Transactions of the ASME, Vol.112, April 1990, pp. 144-150.

27. Catlow, M. G., and Walls, G. W., "A Study of Stress Distribution in Pirns," Journal of the Textile Institute, Transactions, Vol.53, №9, pp. T410-429 (1962).

28. Connolly, D., and Winarski, D. J., "Stress Analysis of Wound Magnetic Tape," Triblogy and Mechanics of Magnetic Storage Systems, ASLE Special Publication SP-16, pp. 172-182 (1984).

29. Frye, K. G., "Winding Variables and Their Effect on Roll Hardness and Roll Quality," TAPPI Journal, Vol.50, №7, pp. 81A-86A (1967).

30. Hanisch, K., "Stress and Strain in Coils of Wound Foils," Journal of Theoretical and Applied Mechanics, Vol.4, №1, pp. 59-72 (1985).

31. Harland, W. G., "Stress Distribution and Winding Faults in Reels of Plastic Film," Polymer Engineering and Science, Vol.7, №1, pp. 59-62 (1967).

32. Hussein, S. M., and Farrell, W. R., "Roll Winding - Causes, Effects and Cures of Loose Cores in Newsprint Rolls," TAPPI Journal, Vol.60, №5, pp. 112-114 (1977).

33. Hussein, S. M., Farrell, W. R., and Gunning, J. R., "Most Paper in the Roll is in Unstable Condition," Canadian Pulp and Paper Industry, Vol.21, №8, pp. 52-53 & 61 (1968).

34. Rand, T., and Eriksson, L. G., "Physical Properties of Newsprint Rolls During Winding," TAPPI Journal, Vol.56, №6, pp. 153-156 (1973).

35. Eriksson, L. G., Lydig, C., and Viglund, J. A., "Measurement of Paper Roll Density During Winding," TAPPI Journal, Vol.66, №1, pp. 63-66 (1983).

36. Monk, D. W., Lautner, W. K., and McMullen, J. F., "Internal Stresses Within Rolls of Cellophane," TAPPI Journal, Vol.58, №8, pp. 152-155 (1975).

37. Southwell, R. V., An Introduction to the Theory of Elasticity for Engineers and Physicists, London: Oxford University Press, 1936.

38. Urmanskii, E. S., Kryuchkov, V. V., and Rakovskii, V. A., "Determination of the Stressed State of a Coil of Magnetic Tape," Strength of Materials, Vol.10, №3, pp. 332-335 (1978) (in English).

39. Urmanskii, E. S., Kryuchkov, V. V., and Shidlovskii, N. S., "Estimating the Effect of the Temperature Factor on the Bearing Capacity of a Reel of Magnetic Tape," Strength of Materials, Vol.13, №8, pp. 1011-1015 (1982) (in English).

40. Urmanskii, E. S., Kryuchkov, V. V., and Shidlovskii, N. S., "Supporting Capacity of Roll Polymer Films," Strength of Materials, Vol.12, №10, pp. 1294-1305 (1981) (in English).

41. Urmanskii, E. S., and Shidlovskii, N. S., "Experimental Study of Residual Stresses in Reels of Magnetic Tape," Strength of Materials, Vol.15, №10, pp. 1402-1409 (1984) (in English).

42. Yablonskii, B. V., "Stress State of a Multilayer Construction in the Winding of a Band on a Cylinder," Soviet Applied Mechanics, Vol.7, №2, pp. 225-227 (1973) (in English).

43. Perkins, R. W., and Mark, R. E., "On the Structural Theory of the Elastic Behavior of Paper," TAPPI Journal, Vol.59, №12, pp. 118-120 (1976).

44. Kimura, M., and Shimizu, H., "Stress and Strain Analysis of a Rectangular Specimen in Elongation Testing," TAPPI Journal, Vol.67, №4, pp. 128-131 (1984).

45. Baum, G. A., Brennan, D. C., and Habeger, C. C., "Orthotropic Elastic Constants of Paper," TAPPI Journal, Vol.64, №8, pp. 97-101 (1981).

46. Prud'homme, R. E., and Robertson, A. A., "Composite Theories Applied to Oriented Paper Sheets," TAPPI Journal, Vol.59, №1, pp. 145-148 (1976).

47. Senko, E., and Thorpe, J., "On-Line Ultrasonic Measurement of Sheet Modulus," TAPPI Journal, Vol.68, №2, pp. 95-99 (1985).

48. Baum, G. A., Pers, K., Shepard, D. R., and Ave'Lallemant, "Wet Straining of Paper," TAPPI Journal, Vol.67, №5, pp.100-104 (1984).

49. Shigley, J. E., and Mitchell, L. D., Mechanical Engineering Design, 4th Edition, McGraw-Hill Book Company, 1983.

50. Elias, T. C., "Investigation of the Compression Response of Ideal Unbounded Fibrous Structures," TAPPI Journal, Vol.50, №3, pp. 125-132 (1967).

51. Ramasubramanian, M. K., and Perkins, R. W., "Computer Simulation of the Uniaxial Elastic-Plastic Behavior of Paper," Transactions of the ASME (Journal of Engineering Materials and Technology), Vol.110, pp. 117-123, (April 1988).

52. Mullins, L., "Engineering with Rubber," CHEMTECH, pp. 720-727 (December 1987).

53. Mises, R. V., "On Saint Venant's Principle," Bull. Amer. Math. Soc., Vol.51, pp. 555-562, (1954).

54. Sternberg, E., "On Saint-Venant's Principle," Quarterly of Applied Mathematics, Vol.11, pp. 393-402, (1954).

55. Diltz, J. L., "How to Avoid Core Spin-Out," PIMA, Vol.67, pp. 44-45, (February 1985).

56. Kratena, J., "A Contribution to the Solution to the Stress State of Webs of Small Depth-to-Thickness Ratios Subjected to Uniform Partial Edge Loading," ACTA TECHNICA CSAV, №1, pp. 98-107 (1978).

57. Provan, J. W., Stress Analysis, Department of Mechanical Engineering, McGill University, December 1988.

58. Bach, G. G., Tensor Analysis and Applications, Department of Mechanical Engineering, McGill University, October 1979.

59. Bach, G. G., Applied Mathematics, Department of Mechanical Engineering, McGill University, October 1979.

60. Bach, G. G., Numerical Analysis, Department of Mechanical Engineering, McGill University, September 1982.

61. Love, A. E. H., A Treatise of the Mathematical Theory of Elasticity, 4th Edition, Dover Publications, New York, 1944.

62. Kaplan, W., Ordinary Differential Equations, 1958 (4th Printing August 1962).

63. Crandall, S. H., Dahl, N. C., and Lardner, T. J., An Introduction to the Mechanics of Solids, 2nd Edition.

64. Lekhnitskii, S. G., Theory of Elasticity of an Anisotropic Elastic Body, (Translated by Fern, P.), Holden-Day, Inc., San Francisco, 1963.

65. Lekhnitskii, S. G., Anisotropic Plates, (Translated by Tsai, S. W., and Cheron, T.), Gordon and Breach Science Publishers, 1968.

66. Edwards, C. H., and Penney, D. E., Calculus and Analytic Geometry, Prentice-Hall, Inc., New Jersey, 1982.

67. Leşan, D., Lecture Notes in Mathematics: Saint-Venant's Problem, (Edited by Dold, A., and Eckmann, B.), Springer-Verlag Berlin Heidelberg, Germany, 1987.

68. Timoshenko, S. P., and Goodier, J. N., Theory of Elasticity, 3rd Edition, McGraw-Hill Book Company, 1987.

69. Fried, I., and Johnson, A. R., "Nonlinear Computation of Axisymmetric Solid Rubber Deformation," Computer Methods in Applied Mechanics and Engineering, Vol.67, №2, pp. 241-253 (1988).

70. Lekhnitskiy, S. G., "Effect of Concentrated Forces on Stress Distribution in Anisotropic Elastic Medium," Prikladnaya matematika i mekhanika, Vol.3, №1, 1936.

71. Muskhelishvili, N. I., Some Basic Problems of The Mathematical Theory of Elasticity, Published by the Academy of Sciences of the U.S.S.R., Moscow, 1954.

72. de Saint-Venant, B., Memoirs des Savants Etrangers, Vol.14, 1855.